Cell Reports

Article

Early time window for memory ensemble allocation specifically depending on activity in Syt2+ early-born parvalbumin interneurons

Graphical abstract

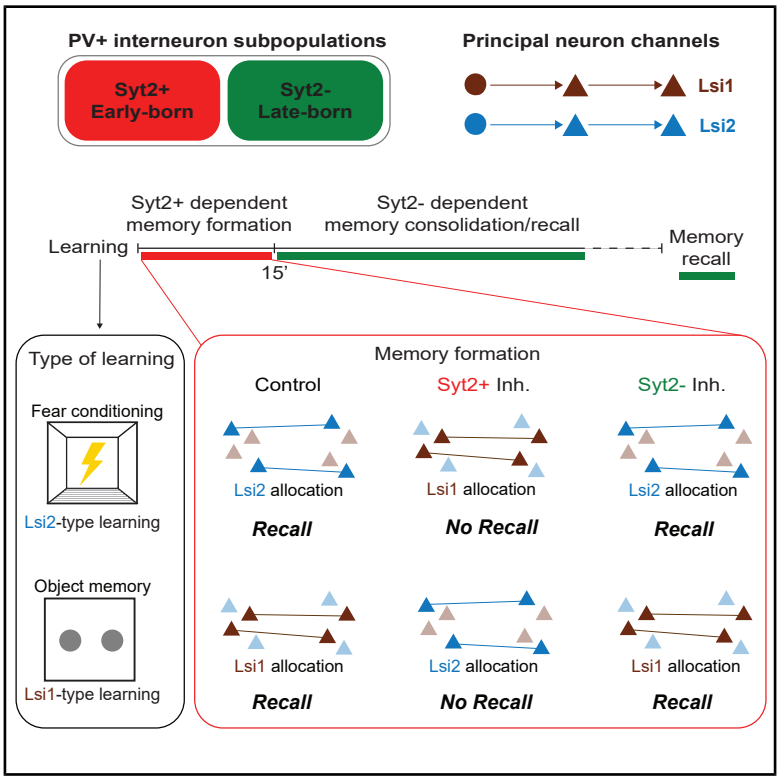

Highlights

- Early- and late-born parvalbumin neurons targeted separately using *Syt2-Cre* mice
- Syt2+PV+ early-born interneurons are required for early memory formation upon learning
- Syt2−/PV+ late-born neurons are required for later memory consolidation and retrieval
- Memory formation involves allocation of proper PN subpopulation to memory ensemble

Authors

Sergio Valbuena, Komal Bhandari, Annapoorani Udhayachandran, Matteo Tripodi, Pico Caroni

Correspondence

caroni@fmi.ch

In brief

Valbuena et al. investigate how parvalbumin (PV) and principal neuron (PN) subpopulations affect hippocampal memory formation and consolidation. They show that Syt2+PV+ interneurons are required during an early time window to allocate the proper PN subpopulation to forming memory ensembles, whereas Syt2−/PV+ are required subsequently to consolidate and retrieve memories.

Valbuena et al., 2025, Cell Reports *44*, 116144
August 26, 2025
https://doi.org/10.1016/j.celrep.2025.116144

CellPress

Cell Reports

CellPress
OPEN ACCESS

Article

Early time window for memory ensemble allocation specifically depending on activity in Syt2+ early-born parvalbumin interneurons

Sergio Valbuena,[1,5] Komal Bhandari,[1,2,5] Annapoorani Udhayachandran,[1,3,5] Matteo Tripodi,[1,4] and Pico Caroni[1,6,*]
[1]Friedrich Miescher Institute for Biomedical Research, Basel, Switzerland
[2]Max Planck Institute of Psychiatry, Munich, Germany
[3]Max Delbrueck Center for Molecular Medicine, Berlin, Germany
[4]Epigenetics and Neurobiology Unit, European Molecular Biology Laboratory, Monterotondo, Italy
[5]These authors contributed equally
[6]Lead contact
*Correspondence: caroni@fmi.ch
https://doi.org/10.1016/j.celrep.2025.116144

SUMMARY

In learning and memory, the encoding of experience is converted into memory ensembles, affecting future behavior. The mechanisms underlying such memory formation are poorly understood, but parvalbumin-expressing (PV) interneurons might be important due to their roles in shaping offline network activity. Here, we addressed the roles of early- and late-born PV neuron subpopulations in memory formation and consolidation in mice. Subpopulation-specific silencing of early-born Syt2+ hippocampal PV neurons during an early 15-min time window upon learning prevented allocation of cFos expression to the correct learning-related principal neuron (PN) subpopulation and memory formation. Conversely, late-born Syt2− PV neurons were specifically required for subsequent memory consolidation and recall, but not PN allocation. During memory formation, the recruitment of one PN subpopulation prevented the subsequent recruitment of the alternative subpopulation. Therefore, memory ensemble allocation to the correct PN subpopulation is a critical early step in memory formation, specifically depending on the activity of Syt2+ early-born PV neurons.

INTRODUCTION

Learning and memory are distinct but intimately interconnected processes. In a key early step (memory formation), online encoding of experience (i.e., acquisition) is translated into neuronal ensembles that will provide memory traces of that experience.[1–5] The principles and mechanisms underlying this early transition from experience to memory ensemble allocation are poorly understood. The requirements unique to memories include retrieval specificity, opposite needs for diversification and generalization, updates through new learning, and prioritization. How these requirements are implemented through memory ensembles is currently unclear, but specific offline network activity processes, partly re-evoking recent experiences, are involved in initial ensemble allocation (memory formation) and subsequent memory consolidation processes.[6–9] The network processes depend critically on the activity of inhibitory interneurons.[10,11] Among them, parvalbumin (PV)-expressing interneurons ensure specificity and binding in memories and are involved in memory consolidation through their selective network synchronization roles.[12–17]

Memory formation and consolidation involve cascades of specific network activity, signal transduction, and gene expression processes, whose unfolding begins after online acquisition and proceeds up to a time window of 12–15 h after acquisition when long-term memory consolidation is completed.[9,18–21] At the level of individual neurons, ensemble formation and consolidation are influenced by intrinsic excitability and involve cellular and synaptic plasticity processes.[22–34] In parallel, forming memory ensembles are shaped and consolidated through offline oscillatory network activities in the theta and gamma range as well as through sharp-wave ripples.[6,9] Whether, at the individual neuron as well as at the network level, these complex memory formation and consolidation processes involve recruitment of specific subpopulations of principal neurons (PNs) and/or interneurons has remained unclear.

Local PNs recruited into memory ensembles in the amygdala and the hippocampus can exhibit enhanced intrinsic excitability.[1,2,25,28,33] Which neurons are most excitable at any given time can be subject to drift, providing a potential mechanism for shifting recruitment to distinct memory ensembles at different times.[8,31,35] In addition, PNs differ in their timing of neurogenesis, which leads to the generation of PN subpopulations exhibiting selective connectivity among interconnected neurons of the same relative age.[36–38] In one case, the existence of PN subpopulations was revealed and leveraged through the use of *Thy1* promoter-driven transgenic mice, in which the two lines Lsi1 and Lsi2 label PN assembling into parallel, selectively connected

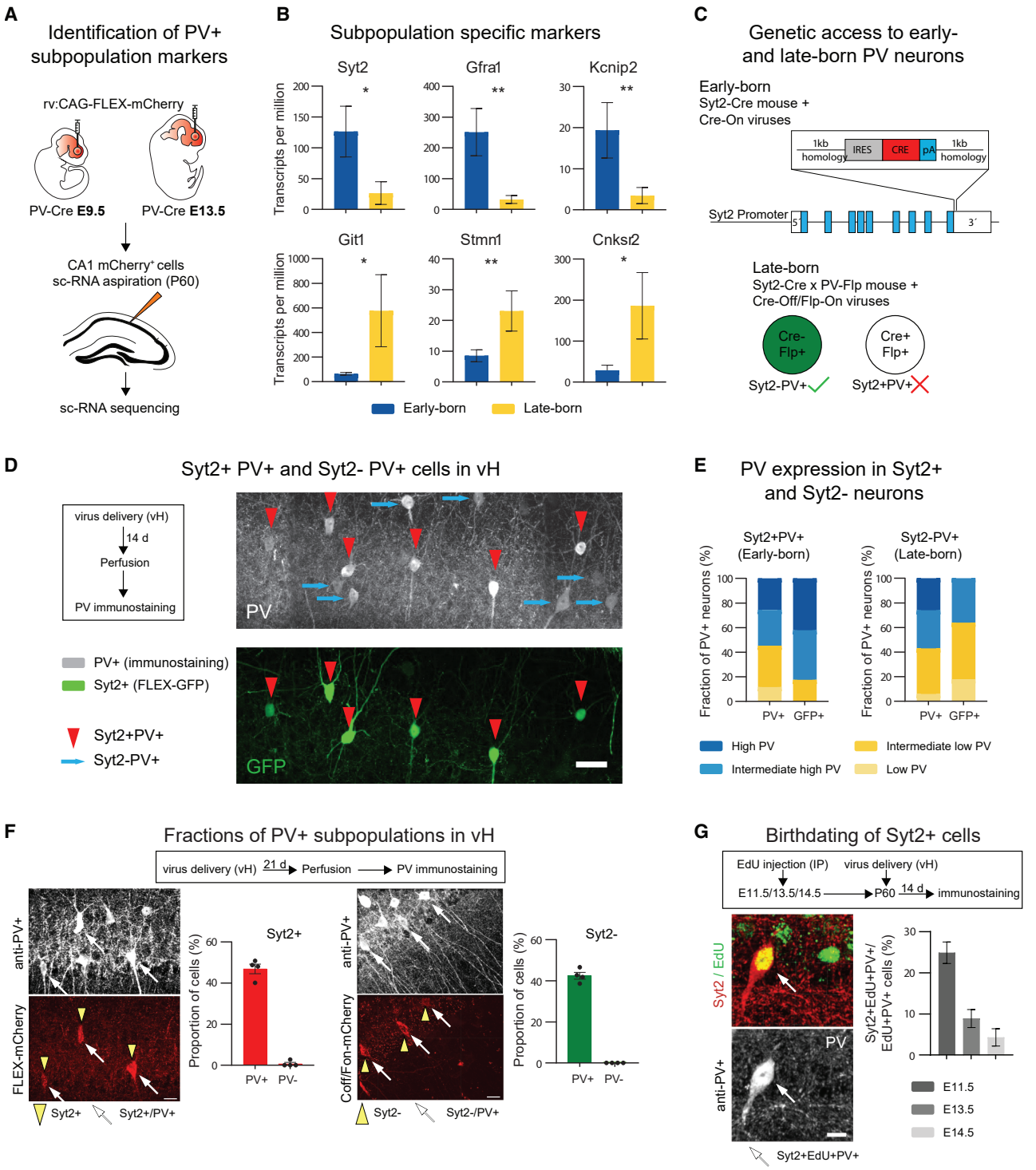

Figure 1. Targeting early- and late-born PV interneuron subpopulations through Syt2 expression

(A) Identification of PV+ subpopulation markers based on their dates of birth.

(B) Expression of subpopulation-specific markers in adult early- and late-born PV neurons.

(C) Genetic access to early-born (*Syt2-Cre* mice) and late-born (*Syt2−Cre−* and *PV−Flp+* mice) PV+ neurons.

(D) Immunocytochemical visualization of Syt2+ and Syt2−PV+ neurons in vH(CA1). AAV-mediated Cre-dependent expression of GFP in *Syt2-Cre* mice. Scale bars, 20 μm.

(E) PV expression levels in hippocampal Syt2+ and Syt2− PV+ neurons.

(legend continued on next page)

circuits throughout and beyond hippocampal loops.[36] Each of these two PN subpopulations accounts for about 20%–25% of total local PNs, and both are generated relatively early during hippocampal PN neurogenesis.[36] Hippocampal PNs sharing a neurogenesis time window tend to fire together in the adult,[38] but how the parallel circuits differ from each other and whether the PN subpopulations can be recruited selectively to memory ensembles has remained unclear. Likewise, PV interneurons consist of two subpopulations of comparable relative size generated at different times during neurogenesis (early-born PV [ePV] and late-born PV [lPV] neurons[39]). The PV neuron subpopulations differ in the density of excitatory and inhibitory synapses targeting the PV neuron somas and proximal dendrites and in how they exhibit plasticity upon changes in excitation or inhibition or different forms of learning.[39,40] While the activity of PV neurons is critically important throughout memory formation and consolidation,[20] whether and how the PV subpopulations have distinct roles in these processes and how they interface with the PN subpopulations have remained unclear.

Here, we address the roles of ePV and lPV+ neuron subpopulations in hippocampal memory formation and consolidation. We found that memory formation depends specifically on the activity of early-born Synaptotagmin 2+ (Syt2+) (and not late-born Syt2−) PV+ neurons during an early time window of about 15 min upon acquisition. The early Syt2+-dependent time window was followed by Syt2− (and not Syt2+)-dependent memory consolidation and retrieval. We further found that different forms of learning (provisional versus definite[40]) involved allocation of cFos+ neurons to either Lsi1 (provisional) or Lsi2 (definite) PNs. Notably, the activity in Syt2+ neurons specifically during the early time window was critical for long-term allocation of the appropriate Lsi1 or Lsi2 subpopulation of PNs to memory ensembles. Taken together, our results determine a specific initial time window for Syt2+-dependent memory formation through allocation of cFos expression to the appropriate PN subpopulation.

RESULTS

Targeting ePV and lPV interneuron subpopulations through Syt2 expression

To determine whether ePV and lPV neurons might reflect subpopulations distinguishable by the expression of distinct genes and, hence, targetable genetically, we carried out a single-cell RNA sequencing differential expression analysis of adult mouse PV neurons born at either embryonic day (E) 9.5 (ePV neurons) or E13.5 (lPV neurons). Embryos from homozygous PV-Cre mice were injected with Cre- and replication-dependent mCherry-expressing retrovirus (rv-FLEX-mCherry) at E9.5 or E13.5, and dorsal hippocampus (dH) slices were prepared from adult mice[41] (Figure 1A). Somatic cytosols of mCherry-expressing neurons were extracted and processed for mRNA analysis, and data from E9.5 and E13.5 postmitotic PV neurons were compared (Figure 1A). A detailed account of the procedure used,[42] including related quality controls, can be found in the STAR Methods.

While many genes were expressed at comparable levels in ePV and lPV neurons, some genes consistently exhibited major differences in expression levels (Figures 1B and S1A). Consistent with the results of previous studies, ePV neurons exhibited higher levels of the gamma-aminobutyric acid (GABA) synthesizing enzyme *Gad1*, whereas they only expressed slightly elevated levels of the PV transcript, suggesting that the robust differences detected by PV immunocytochemistry arise post transcriptionally[39] (Figure S1A). Among differentially expressed genes, *Gfra1*, *Syt2*, and *Kcnip2* were expressed in ePV neurons at levels more than 7-, 4-, and 9-fold, respectively, higher than in lPV neurons (Figure 1B). Conversely, *Git1*, *Stmn1*, and *Cnksr2* were expressed in lPV neurons at levels more than 8-, 3-, and 6-fold, respectively, higher than in ePV neurons (Figure 1B). Further differentially expressed genes included *Nefm*, *Nefh*, *Vamp1*, *Atp1a3*, *Gria1*, and *Caln1* (higher expression in ePV) and *Mapk1*, *Fmn2*, and *Lrrc7* (higher expression in lPV) (Figure S1A). Therefore, ePV and lPV subpopulations exhibit pronounced gene expression differences, supporting the notion that they reflect distinct subpopulations of neurons.

To target ePV neurons genetically, we generated *Syt2-Cre* mice (Syt2+ mice; Figure 1C). The mice allowed expression of Cre-dependent reporters as well as chemogenetic and optogenetic tools from the *Syt2* locus (Figures 1C and 1D). While *Syt2-Cre* mice allowed targeting of PV neurons in the dH and ventral hippocampus (vH), most of our subsequent analyses focused on vH due to its advantages in targeting behavioral functions. As expected, genetically marked Syt2+ PV neurons represented a substantial fraction (about half; Figure 1F) of total vH PV neurons and, on average, expressed higher levels of PV protein than the general population of PV neurons[39] (Figures 1D–1F and S1C). To target Syt2− PV neurons (lPV), we employed an intersectional approach involving crosses of *Syt2-Cre* and *PV-Flp* mice, combined with Cre-OFF/Flp-ON viruses to exclude Syt2+ cells from the manipulation[43,44] (Figures 1C–1F). Both Syt2+- and Syt2−-targeted neurons in vH were almost exclusively PV+ (Figure 1F). As predicted, early-born neurons accounted for most genetically marked Syt2+PV+ neurons in vH and dH, whereas most lPV+ neurons were not targeted in *Syt2-Cre* mice (Figure 1G). Furthermore, hippocampal early-born neurons expressed Syt2, whereas most late-born neurons did not (Figure S1B). Therefore, *Syt2-Cre* mice provide a valuable tool to directly target hippocampal early-born Syt2-expressing PV+ neurons and indirectly target late-born Syt2−PV+ neurons using an intersectional approach involving crosses of *Syt2-Cre* and *PV-Flp* mice, combined with Cre-OFF/Flp-ON viruses.

(F) Fractions of Syt2+ and Syt2− subpopulations and extent of overlap with PV+/PV− cells in vH. Left, immunocytochemical visualization of PV+ neurons (top; white arrows) and Syt2+ cells labeled with a fluorescent reporter (bottom; yellow arrowheads: Syt2+PV+); quantification of the proportion of PV+ and PV− cells that are Syt2+. Right, same for co-localization of PV+ neurons with Syt2− cells. Scale bars, 30 μm.
(G) Birthdating of Syt2+/PV+ cells. Left: immunocytochemical visualization of EdU+ (developmental injection), Syt2+ (fluorescent reporter), and PV+ cells in adult vH. Right: fraction of vH PV+ neurons targeted in *Syt-Cre* mice and labeled with EdU-labeled upon EdU injections at E11.5, E13.5, or E14.5. Scale bars, 10 μm. Exact Mann-Whitney test (A). $p < 0.05$ (*) and $p < 0.01$ (**). $n = 11$ (B), 3 (D), 4 (F), and 3–5 (G). See also Figure S1.

Early time window for Syt2+ PV-dependent memory formation

To determine whether PV neuron subpopulations might have distinct roles for memory formation and consolidation upon learning, we carried out experiments in which Syt2+PV+, Syt2−PV+, or all PV+ neurons were silenced chemogenetically[45] from different time points after contextual fear conditioning (cFC). In some experiments, to achieve better temporal resolution at the onset of the treatment, we used a pharmacologically selective actuator module channel/pharmacologically effective effector molecule ligand (PSAM/PSEM) chemogenetic system in which inhibition is detected 1–2 min upon delivery of PSAM and lasts for about 1.5 h[46] (Figure S2A).

Activation of inhibitory designer receptors exclusively activated by designer drugs (DREADD) in Syt2+ neurons with clozapine N-oxide (CNO) delivery 15 min after exposure to cFC significantly reduced freezing upon recall in conditioning context on the subsequent day (Figure 2A; see comparable results with PSAM/PSEM system in Figure S2A and the corresponding virus and ligand controls in Figure S2C). To assess the extent of vH-dependent cFC memory reduction upon Syt2+ neuron inhibition 15 min after acquisition, we compared the freezing values obtained upon inhibition of Syt2+ PV neurons in vH to those obtained in experiments in which the activator of GABAergic transmitter muscimol was used to locally inhibit the activity in vH or dH at recall of cFC[47] (Figure 2B). Inhibiting vH at recall 1 day after cFC with muscimol reduced freezing to an extent closely comparable to inhibiting Syt2+ neurons from 15 min after acquisition (Figure 2B). By contrast, inhibiting dH at recall with muscimol had no detectable impact on freezing to context upon cFC (Figure 2B). We hypothesized that this finding might indicate that the contribution of dH to freezing upon cFC might be masked by a much larger contribution by vH. Indeed, inhibiting dH at recall with muscimol in mice in which vH Syt2+ neurons had been inhibited at 15 min after acquisition abolished freezing (Figure 2B; for inhibition of vH and dH with muscimol or DREADD see also ref.[48]). In control experiments, we obtained closely comparable results when using the Cre-on/Flp-on system to target Syt2+ neurons 15 min after acquisition or when waiting for 28 days instead of 10 days between virus injections and the beginning of the inhibition experiments (Figures S2D and S2E). Taken together, these results suggested that inhibiting vH Syt2+ neurons chemogenetically at 15 min after acquisition effectively suppresses the formation of vH-dependent cFC memory as detected at recall.

Unlike Syt2+ inhibition at 15 min, inhibition of Syt2+ neurons 3 h after acquisition, at a time when PV neuron activity is still important for memory consolidation (Karunakaran et al.[20]; Figure 2A), had no detectable effect on freezing at recall (Figures 2A and S2F). Likewise, Syt2+ neuron inhibition at 7 h (outside of PV neuron-dependent memory consolidation time windows[20]), at 12 h (inside late time window for PV-dependent memory consolidation), or at recall had no impact on freezing at recall (Figures 2A and S2F). Notably, and in stark contrast to Syt2+ inhibition, inhibition of vH Syt2-neurons at 15 min after acquisition of cFC had no effect on freezing at recall, whereas Syt2-inhibition at 3 h, 12 h, or at recall suppressed vH-dependent freezing at recall of cFC (Figures 2A and S2F). As might have been predicted,[20] inhibiting all vH PV neurons at 15 min, 3 h, 12 h, or at recall (but not at 7 h after acquisition) suppressed vH-dependent freezing (Figures 2A and S2F). Taken together, these results indicated that memory formation in vH after cFC acquisition depends specifically on activity in Syt2+ but not Syt2− PV neurons 15 min after acquisition, whereas it specifically depends on activity in Syt2− but not Syt2+ PV neurons at 3 h or 12 h after acquisition as well as at recall.

To better define the time window depending on the activity in Syt2+PV+ neurons, we carried out experiments in which chemogenetic inhibition of Syt2+PV+ neurons was triggered with CNO or PSEM delivery at different time points after acquisition of cFC. These experiments indicated that the time window during which memory formation depends on the activity in Syt2+ neurons extends from 10 min (earliest time point tested) to before 20 min after acquisition, whereas Syt2+ inhibition from 20 min onwards had very little (20 and 30 min) or no (90 min) detectable impact on vH-dependent memory at recall (Figures 2C and S2A). The duration of the time window for Syt2+-dependent memory formation was confirmed in experiments in which Syt2+ neurons were inhibited through light-mediated optogenetic inhibition (Figure 2D). Therefore, vH-dependent memory formation is specifically dependent on the activity of Syt2+ (but not Syt2−) PV neurons from about 5 min until about 15 min (but not 20 min) after acquisition of cFC.

To determine whether the early time window for Syt2+-dependent memory formation also applies to forms of learning not depending on vH, we carried out similar Syt2+ inhibition experiments after extinction of cFC, a form of learning that depends on activity in dH (but not vH; Figure S2G) and involves the induction of plasticity in lPV neurons (instead of ePV neurons upon cFC[39]) (Figure 2E). Like in cFC, inhibition of dH Syt2+ PV neurons (or of all dH PV neurons) 15 min after extinction learning suppressed extinction memory as detected 24 h later at retention, whereas inhibition of all dH PV neurons (but not specifically Syt2+ PV neurons) suppressed extinction memory when carried out 3 h after extinction learning (Figure 2E). Taken together, these results provide evidence of the existence of an early time window for Syt2+-dependent fear and extinction memory formation up to 15 min after learning, which is followed by memory consolidation and recall depending on the activity of Syt2− PV neurons (Figure 2F).

Value-related early closing of time window for memory formation

We next determined whether there might also be an early Syt2+-dependent time window for memory in learning processes not involving reinforcement or learning-related PV neuron plasticity. To address this question, we carried out familiar object recognition (FOR; also known as novel object recognition) experiments, in which, unlike cFC or its extinction, FOR does not involve PV neuron plasticity[40] (Figure 3A). On day 2 of the FOR protocol, mice recognize the familiar object and selectively explore the novel object to an extent comparable to how they explored any of the two previous (at that time novel) objects on day 1 (Figure S3A). Inhibition of vH Syt2+ PV neurons 15 min after first exposure on day 1 suppressed FOR memory on day 2, as

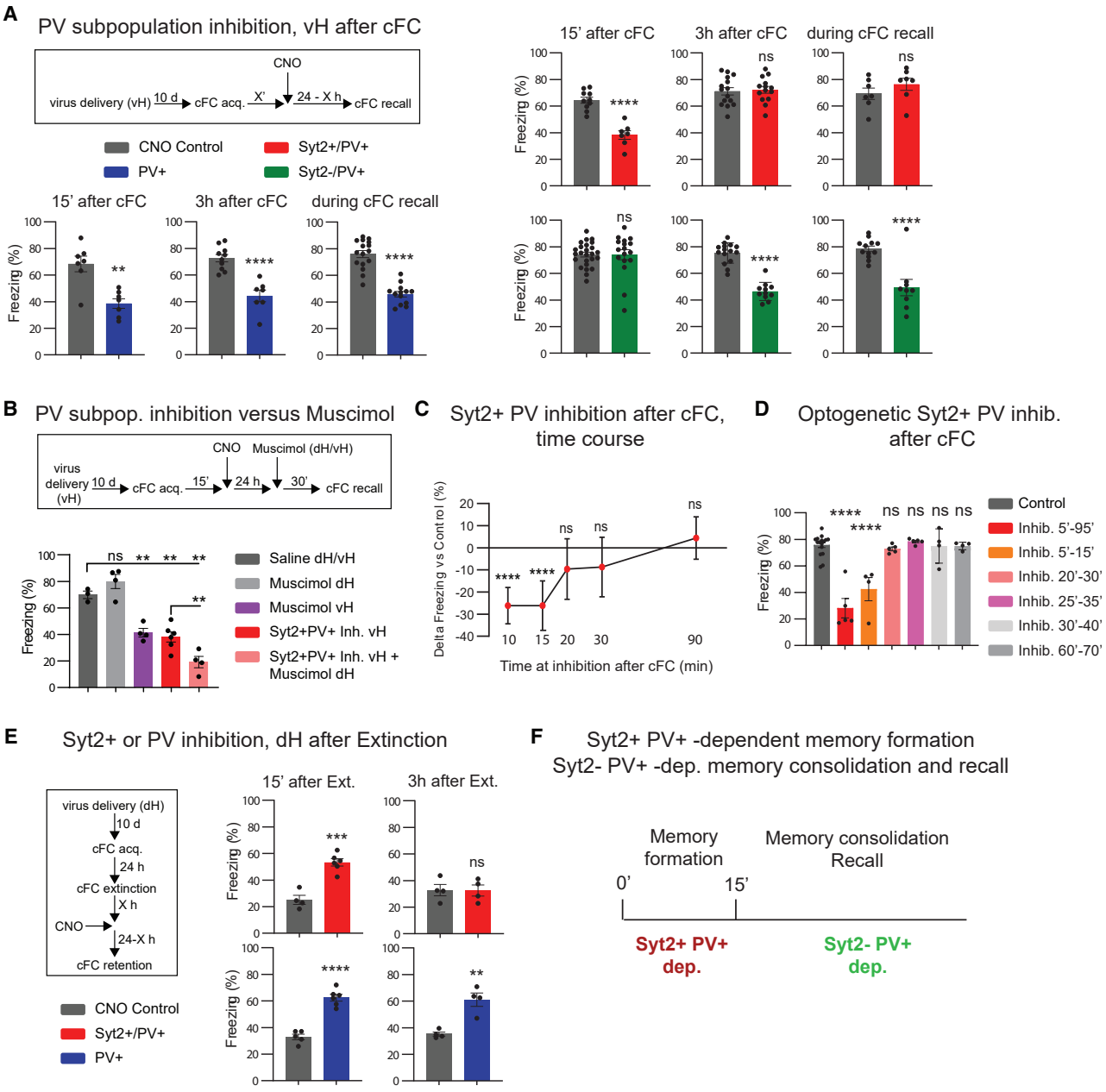

Figure 2. Early time window for Syt2+ PV-dependent memory formation

(A) Impact of vH chemogenetic PV subpopulation inhibition at 15 min and 3 h after acquisition (or at recall) of cFC on freezing at recall.

(B) Chemogenetic inhibition of vH Syt2+ PV neurons 15 min after acquisition of cFC mimics vH inhibition at recall with muscimol, abolishing vH fear memory.

(C) Time window for sensitivity of cFC memory formation to Syt2+ PV inhibition.

(D) Optogenetic inhibition of vH Syt2+ neurons at 5–15 min after acquisition interferes with cFC memory formation.

(E) Interference with memory formation of extinction learning by inhibition of dH Syt2+ PV neurons 15 min but not 3 h after acquisition.

(F) Early time window for Syt2+ PV-dependent memory formation, followed by Syt2− PV-dependent memory consolidation and recall. Unpaired Student's t test (A, C, and E). $p < 0.01$ (**), $p < 0.001$ (***), and $p < 0.0001$ (****). Ordinary two-way ANOVA followed by Tukey's multiple comparisons post-hoc test (B). $p < 0.01$ (**). Ordinary one-way ANOVA followed by Dunnett's multiple comparisons post-hoc test (D). $p < 0.0001$ and $F = 21.66$. $p < 0.0001$ (****). $n = 6–25$ (A), 3–6 (B), 5 (C), 4–16 (D), and 4–6 (E). See also Figure S2.

indicated by an absence of discrimination between exploration of the familiar or novel object (Figure 3A). In contrast to cFC and extinction, Syt2+ inhibition at 3 h after acquisition also suppressed FOR memory on the next day (Figure 3A). Notably, and in parallel to the extended duration of Syt2+ PV neuron sensitivity, inhibition of Syt2− PV neurons at 15 min or 3 h time point

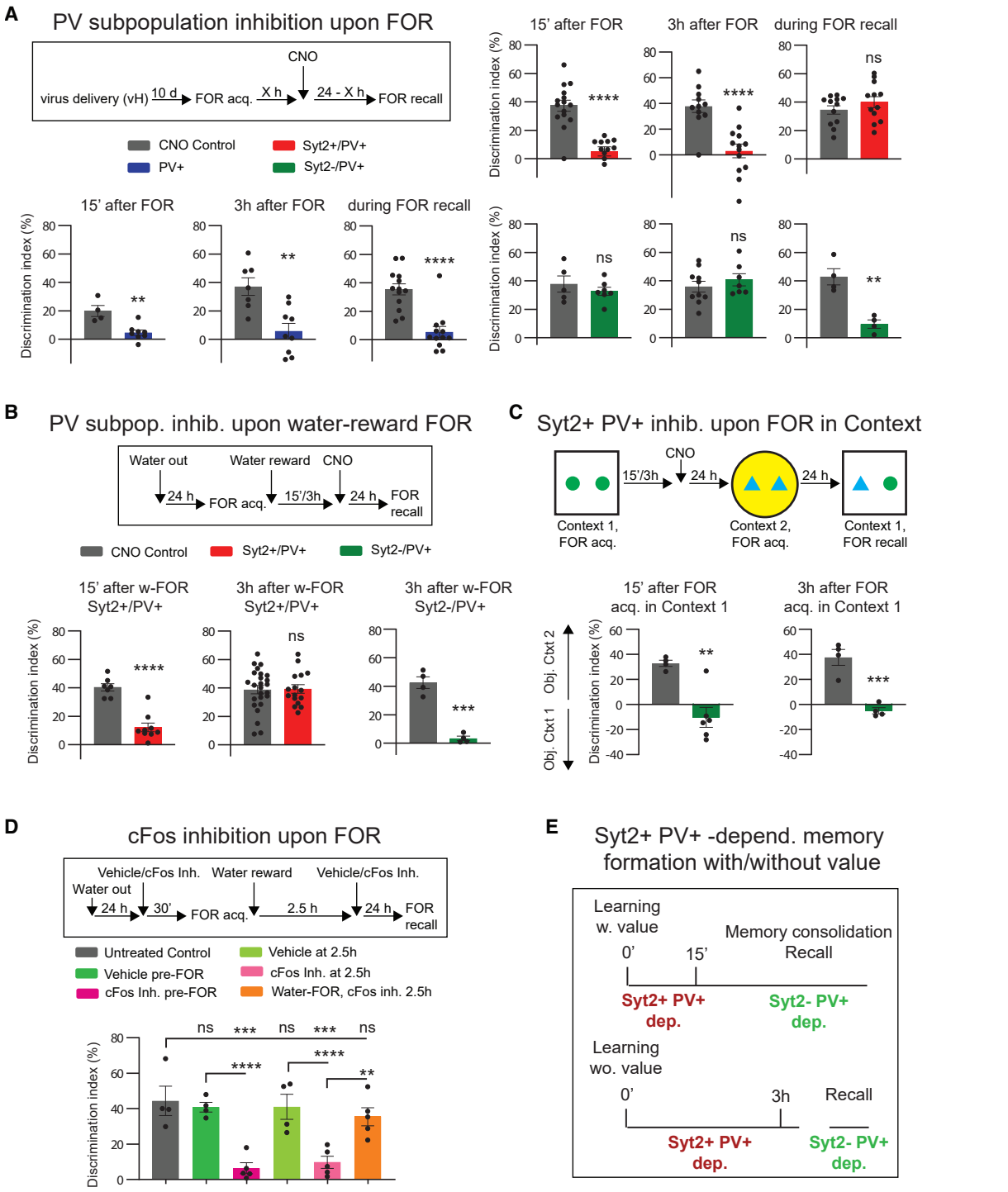

Figure 3. Value-related early closing of time window for memory formation

(A) Inhibition of vH Syt2+ (and not Syt2−) PV neurons 15 min or 3 h after acquisition of FOR specifically interferes with FOR memory at recall.

(B) Associating FOR acquisition with water-reward shortens the Syt2+-dependent time window in FOR.

(C) Inhibition of vH Syt2+ (and not Syt2−) PV neurons 15 min or 3 h after acquisition of FOR in context (context 1) specifically interferes with FOR memory at recall.

(D) Memory formation in FOR, but not in water-FOR, is suppressed by delivery of cFos inhibitor 2.5 h after acquisition.

(E) Extended Syt2+-dependent and Syt2−-independent time window for memory formation in FOR in the absence of association to value (water reward). Unpaired Student's t test (A–C). $p < 0.01$ (**), $p < 0.001$ (***), and $p < 0.0001$ (****). Ordinary two-way ANOVA followed by Tukey's multiple comparison post-hoc test. $p < 0.01$ (**), $p < 0.001$ (***), and $p < 0.0001$ (****). n = 4–15 (A), 7–25 (B), 4–6 (C), and 4–5 (D). See also Figures S3 and S4.

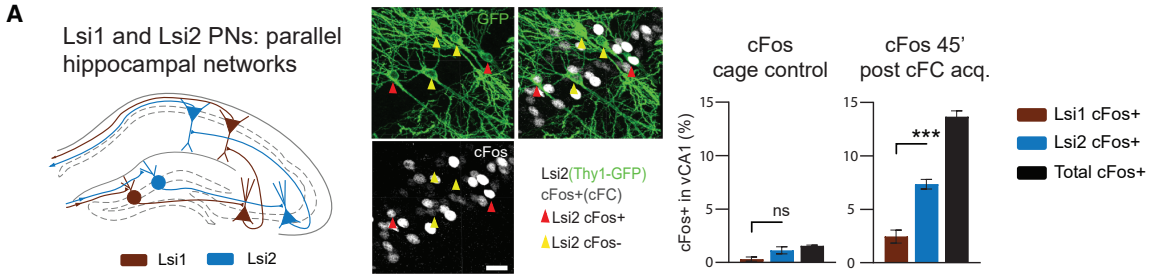

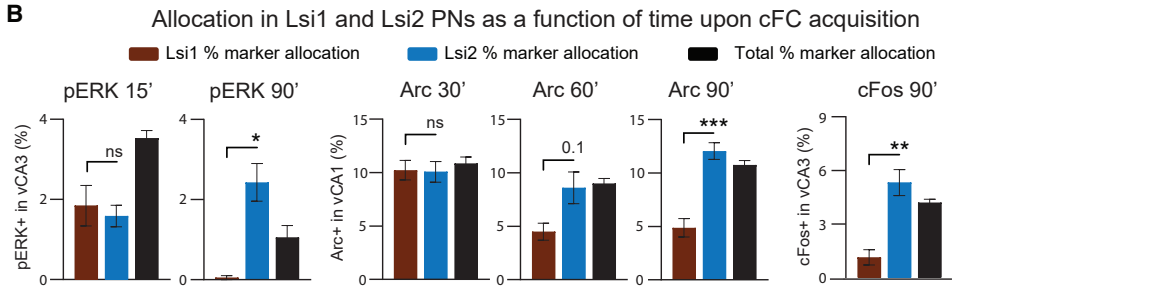

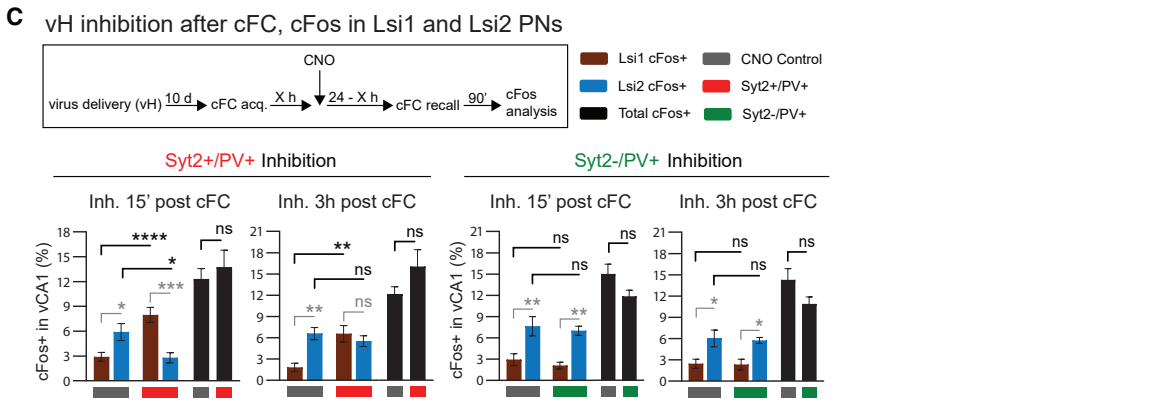

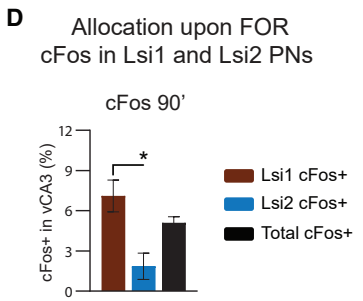

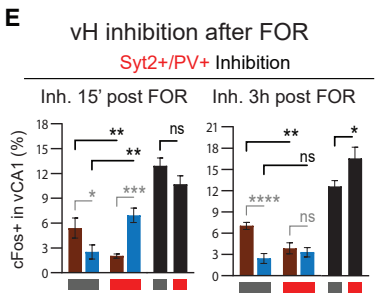

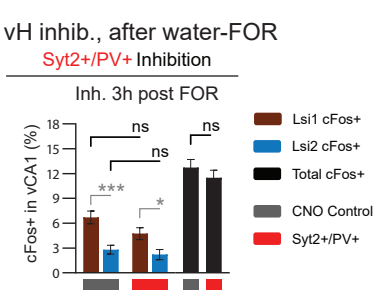

G Specific role of Syt2+ PV neurons for cFos allocation to relevant PN subpopulation

	no PV inh.	Syt2+ inh. *during* formation time window	Syt2+ inh. *after* formation time window *or* Syt2- inh.
cFos in relevant PN subpopulation	++	-/+	++

(legend on next page)

did not affect FOR memory (Figure 3A). Inhibiting Syt2− (but not Syt2+) PV neurons at recall suppressed FOR memory (Figure 3A). In "FOR in context experiments," in which object exploration at testing depended on whether a familiar object was associated with its proper context, the time window for Syt2+-dependent memory formation also extended to 3 h after acquisition (Figures 3C and S3A). Therefore, and unlike cFC or extinction learning, the time window for Syt2+-dependent and Syt2−-independent memory formation extends to up to 3 h after acquisition of FOR.

To determine whether the extended Syt2+-dependent time window for memory formation in FOR might relate to the fact that FOR acquisition does not involve any type of reinforcement, we devised an experimental protocol in which FOR acquisition was associated with positive reinforcement. Mice were water deprived for 24 h before FOR acquisition and provided with water access at the end of the 10-min FOR acquisition session, thereby associating the episode of memory acquisition in FOR with subsequent positive experience (water-reward version of the FOR protocol; Figure 3B). In the water-reward version of the FOR protocol, inhibition of Syt2+ PV neurons interfered with FOR memory when delivered at 15 min but not at 3 h after acquisition (Figures 3B and S3A). In parallel, inhibition of Syt2− PV neurons 3 h after acquisition, which did not affect memory in the regular FOR protocol, interfered with memory in the water-FOR protocol (Figure 3B). Therefore, introducing an element of positive reinforcement to the FOR acquisition protocol was sufficient to shorten the time window for Syt2+-dependent (and Syt2−-independent) memory formation from at least 3 h to about 15 min.

To search for plasticity counterparts of Syt2+-dependent memory formation, we carried out experiments addressing the time at which memory consolidation depends on the function of the immediate-early gene *cFos*. When the inhibitor of cFos function T-5224 was delivered before acquisition, it prevented memory function at recall in cFC and FOR (Figures 3D and S3C). By contrast and consistent with a longer Syt2+ time window in FOR compared to cFC, delivery of the cFos inhibitor 2.5 h after acquisition affected memory recall in FOR but not in cFC (Figures 3D and S3C). Notably, and in parallel with a shortened Syt2+ time window, the cFos inhibitor did not prevent FOR memory recall anymore when delivered at 2.5 h in the water-reward FOR protocol (Figure 3D). Taken together, these results further supported the notion that a Syt2+-dependent time window represents a critical early step in memory formation, preceding a memory consolidation phase that depends on the activity of the immediate-early gene *cFos* (Figure 3E).

vH network activity during Syt2+-dependent memory time window closing

To search for possible network activity counterparts of the Syt2+-dependent time window for memory formation, we carried out experiments in which we monitored oscillatory activity in vH following acquisition of the water-rewarded FOR memory task. We placed multi-channel silicon electrodes in vH and monitored oscillation power values continuously or across 5-min time intervals preceding and following the 15-min time point when the Syt2+ time window ends upon the water-reward version of the FOR task[48–50] (Figure S4A). To adjust for mouse handling, values detected when mice were returned initially to their home cage upon local field potential (LFP) electrode placement (prior to acquisition of the task) were subtracted as a baseline control to obtain a shift in power values (Figure S4A).

The power of vH oscillations, including those in the low- and high-gamma frequency range during a 5-min interval at 8–13 min after acquisition of the water-reward FOR task, i.e., before the end of the Syt2+-dependent time window, was higher than under baseline handling conditions (Figures S4A and S4B). Oscillation power decreased to values below baseline conditions after the 15-min time point (from the 17–22-min interval onward; Figures S4A and S4B). Notably, when Syt2+ PV neurons, but not Syt2− neurons, were inhibited from 15 min onward, the decrease in gamma-power network activity was prevented (Figure S4C). Therefore, experience-related responses in the low and high gamma range by the vH network 15 min after the acquisition of water-reward FOR are specifically influenced by the activity of Syt2+ PV neurons.

Syt2+-dependent selective allocation of cFos+ neurons to proper PN subpopulations

To investigate how inhibiting Syt2+ PV neuron activity might interfere with memory formation, we focused on the expression of cFos in PN subpopulations Lsi1 and Lsi2 that assemble preferentially interconnected parallel subcircuits across the hippocampal loop from dentate gyrus to Cornus Ammonis * (CA3) and on to CA1[36] (Figure 4A). Accordingly, we carried out experiments in which we monitored the appearance of hippocampal Lsi1 (in *Lsi1-GFP* mice) versus Lsi2 (in *Lsi2-GFP* mice)

Figure 4. Syt2+-dependent selective allocation of cFos+ neurons to proper Lsi1/2 subpopulations

(A) Left: schematic representation of selective Lsi1 and Lsi2 PN connectivity along the hippocampal axis. Center: representative image of Lsi2(GFP+) cFos+ and cFos-cells in vH upon cFC. Right: cFos expression under home cage conditions and 45 min after cFC acquisition as percentages of Lsi1, Lsi2, or total NeuN-positive neurons (right). Scale bars, 20 μm.

(B) Equal expression of plasticity markers (pERK, Arc, or cFos proteins) in vH-CA3 Lsi1 and Lsi2 PNs up to 30 min after cFC, followed by selective expression in Lsi2 neurons.

(C) Syt2+ PV neuron inhibition at 15 min after cFC acquisition disrupts selective allocation of vH-CA1 cFos+ neurons to Lsi2 PNs.

(D) Selective allocation of vH-CA3 cFos+ neurons to Lsi1 (and not Lsi2) PNs upon FOR.

(E and F) Syt2+ PV neuron inhibition at 3 h after FOR (E), but not water FOR (F), acquisition disrupts selective allocation of vH-CA1 cFos+ neurons to Lsi1 PNs.

(G) Inhibition of Syt2+PV+ neurons during the early time window for memory formation disrupts the selective allocation of cFos expression to the relevant PN subpopulation. Unpaired Student's t test (A), (B), and (D), markers in Lsi1 versus Lsi2 cell; (C), (E), and (F), total cFos. Ordinary two-way ANOVA followed by Fisher's least significant difference multiple comparison post-hoc test (C, E, F, cFos in Lsi1 and Lsi2 cells). $p < 0.05$ (*), $p < 0.01$ (**), $p < 0.001$ (***), $p < 0.0001$ (****). n = 3–5 (A), 2–4 (B), 3–8 (C), 4 (D), 4–6 (E), and 5–7 (F). See also Figure S5.

A Lsi1 and Lsi2 Mossy fiber terminals post nNOS blockade at P5-7 or P7-9: Analysis in vCA3b

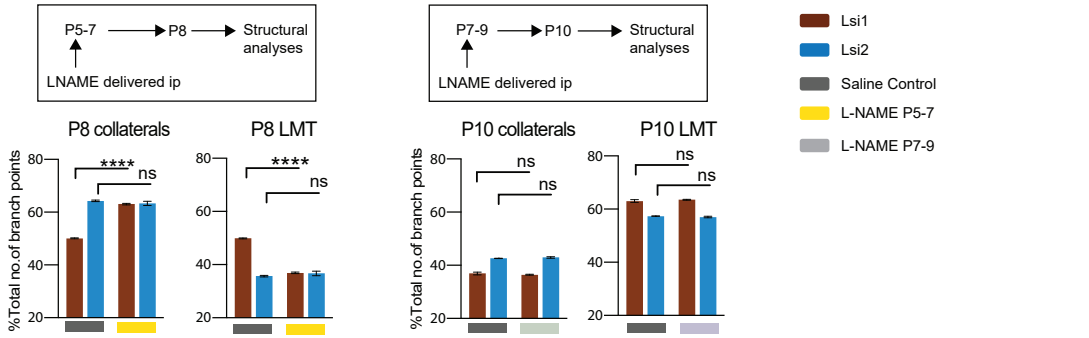

B Connectivity in adult CA3b post nNOS blockade at P5-7: Contacts between DG-LMTs and CA3b PNs

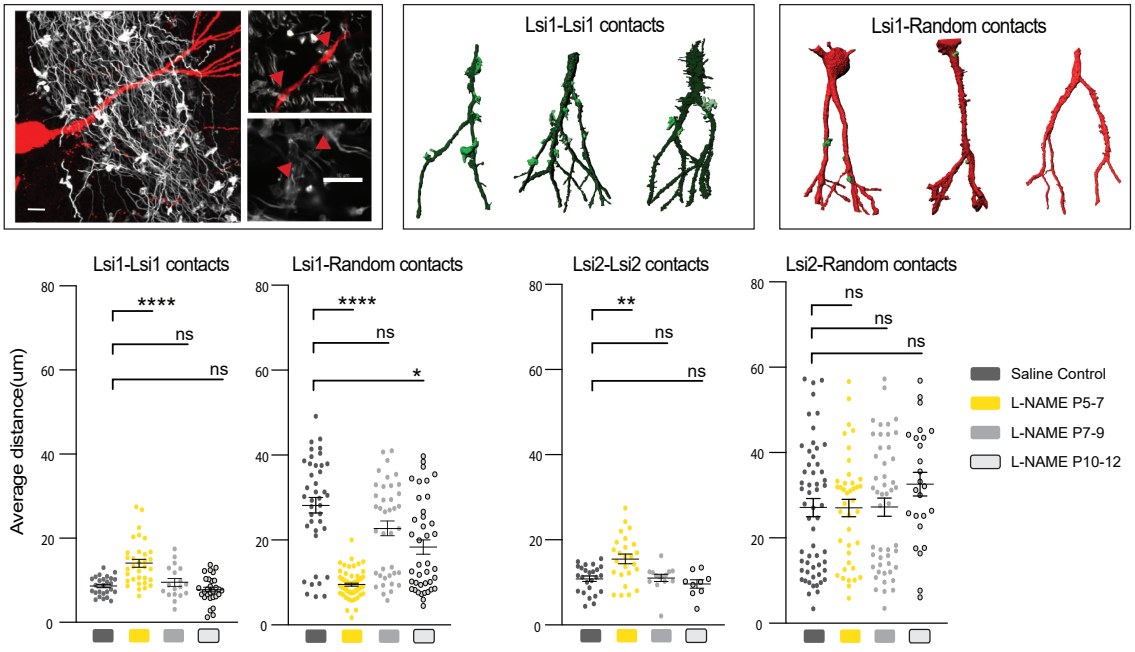

C FOR in the adult, post nNOS blockade at P5-7

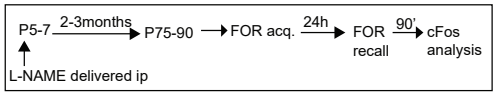

D cFC in the adult, post nNOS blockade at P5-7

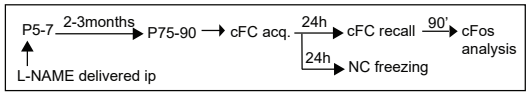

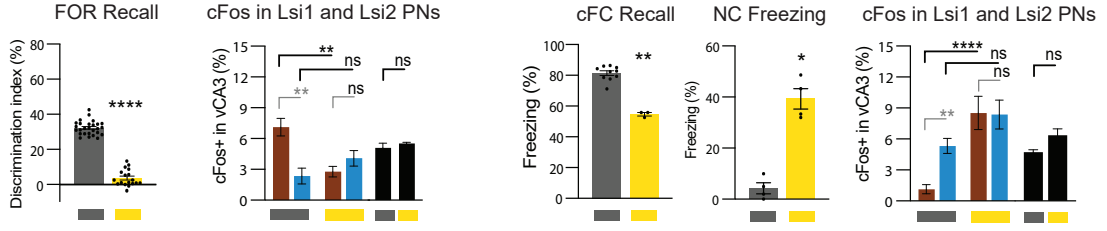

(legend on next page)

expressing cFos+ neurons upon cFC (Figure 4A) or FOR in the presence and absence of activity in Syt2+ PV neurons.

Strikingly, cFC selectively induced cFos expression in vH Lsi2 but not Lsi1 neurons as detected 45 and 90 min upon acquisition as well as at recall (Figures 4A, 4B, and S5D). cFos expression is first detected about 45 min after acquisition,[21] and at that time, expression upon cFC was already selective for Lsi2 neurons (Figure 4A). By contrast, and notably, phosphorylated MAP kinase pERK and phosphorylated CREB were detected equally in Lsi2 and Lsi1 neurons 15 min after acquisition of cFC (Figures 4B and S5A). Furthermore, expression of the plasticity-related early gene *Arc* 30 min after cFC acquisition was detected equally in Lsi1 and Lsi2 neurons, whereas its expression 60 and 90 min after acquisition was selectively detected in Lsi2 neurons (Figure 4B). Therefore, selective allocation of plasticity markers to Lsi2 PNs upon cFC learning (at 45 min) is preceded by initial expression in both Lsi1 and Lsi2 PNs during the early time window for memory formation.

We then carried out experiments in which cFC was followed at the 15 min time point by Syt2+PV+ or Syt2−PV+ (or all PV+) inhibition, followed by detection of cFos expression at 90 min after acquisition or upon recall in Lsi1 (*Syt2-Cre*, *PV-Flp*, *Lsi1* mice) or Lsi2 (*Syt2-Cre*, *PV-Flp*, *Lsi2* mice) neurons (Figures 4C and S5B). Strikingly, selective cFos expression in Lsi2 neurons was lost at recall (or 90 min after acquisition) when Syt2+PV+ neurons or all PV+ neurons, but not Syt2−PV+ neurons, were inhibited 15 min after acquisition of cFC (Figures 4C, S5B, S5D, and S5E). In parallel, Syt2+PV+ neuron inhibition at 15 min after acquisition of cFC led to aberrant expression of cFos in Lsi1 PNs (Figures 4C, S5B, S5D, and S5E). By contrast, inhibition of Syt2+PV+ or Syt2−PV+ neurons at 3 h after acquisition did not prevent cFos expression selectively in Lsi2 neurons upon cFC (Figures 4C and S5B).

We then carried out similar experiments involving the FOR paradigm. Strikingly, FOR acquisition led to the selective expression of cFos in vH Lsi1 but not Lsi2 neurons (Figure 4D). Furthermore, inhibition of vH Syt2+PV+ neurons (or all PV+ neurons) 15 min after FOR acquisition prevented selective allocation of cFos+ neurons to vH Lsi1 (and not Lsi2) PNs at recall of FOR or 90 min after acquisition of FOR (Figures 4E, S5C, S5D, and S5F). As might have been predicted based on the duration of the Syt2+ time window upon unrewarded FOR, inhibition of Syt2+ neurons also interfered with selective allocation of cFos+ neurons to Lsi1 PNs when applied 3 h after acquisition of unrewarded FOR (Figure 4E). Since in these experiments, ensemble sizes as detected by the total fraction of learning-induced cFos+ neurons were not consistently affected by Syt2+ inhibition, these results supported the notion that Syt2+ inhibition and memory disruption specifically involved the prevention of ensemble allocation selectively to the correct Lsi subpopulation.

To further relate the Syt2+ time window for memory formation to selective allocation of cFos+ neurons to the correct Lsi1 subpopulation, we carried out experiments involving the water-reward FOR protocol. Consistent with the shortened time window, Syt2+PV+ inhibition at 3 h in the water-reward version of the FOR did not interfere with selective allocation of cFos expression to Lsi1 neurons (Figure 4F). Taken together, these results provided evidence that the Syt2+ time window for memory formation is closely correlated with stable selective allocation of cFos+ neurons to the correct Lsi subpopulation (Figure 4G), consistent with the notion that the two processes are causally related.

Lsi1-specific cFos dysregulation in mice with selectively disrupted Lsi1 connectivity

To further investigate how interference with memory formation relates to cFos expression in the proper Lsi subpopulation of PNs, we carried out experiments in mice in which selective connectivity within Lsi1 PNs was selectively disrupted during developmental synaptogenesis in hippocampal CA3.[36] In a search for treatments that might selectively interfere with synaptogenesis among one class of Lsi PNs, we found that when a specific inhibitor of nNOS (L-NAME, Nω-Nitro-L-arginine methyl ester hydrochloride), an enzyme with an established role in local signaling for synaptogenesis,[51,52] was delivered to mice during the Lsi1 time window postnatal day (P) P5–7, the treatment specifically delayed synaptogenesis between Lsi1 mossy fibers and Lsi1 CA3 PNs (from collaterals to large mossy fiber terminals [LMTs]; here analyzed in vCA3b; Figure 5A). The same treatment during the Lsi2 time window P7–9 had no impact on Lsi2 or Lsi1 collateral and LMT contacts onto PNs in CA3b as determined at P10 (Figure 5A). Notably, the P5–7 treatment with L-NAME had a dramatic lasting impact on the specificity of connectivity by mossy fibers onto proximal dendrites of PNs in CA3b in the adult (analyzed throughout d-v CA3b; Figure 5B). In addition to more dispersed clusters onto Lsi1 PNs, Lsi1 mossy fibers in P5–7 treated mice imposed clusters of Lsi1 terminals onto non-Lsi1 CA3 PN proximal dendrites (Figure 5B). Consistent with the specificity of the treatment, no major disruption of specificity was detected when Lsi2 mice were treated with L-NAME during

Figure 5. Lsi1-specific cFos dysregulation in mice with selectively disrupted Lsi1 connectivity

(A) Schematic representation of nNOS blockade protocol during Lsi1 and Lsi2 synaptogenesis window in CA3 (top). Lsi1 and Lsi2 mossy fiber terminal collaterals and LMTs in vCA3b as a fraction of total detected mossy fiber branch points in vCA3b stratum lucidum at P8 (L-NAME: P5–7) or P10 (L-NAME: P7–9).

(B) Top, left: representative images of randomly labeled dCA3 PN (red) and mGFP-expressing Lsi1 mossy fibers. Red arrows: randomly labeled dendrites with overlapping mGFP-LMTs. Scale bars, 5 μm. Top, right: representative 3D reconstructions of Lsi1-Lsi1 (middle) and Lsi1-random (right) contacts in dCA3b. Lsi1 LMTs (light green), Lsi1 CA3 PN dendrite (dark green), and randomly labeled CA3 PN dendrite (red). Bottom: quantitative analysis of LMT/PN dendrite contact throughout d-v CA3b stratum lucidum. Each data point represents a single PN in CA3b.

(C and D) Schematic representation of FOR (C) or cFC (D) behavioral protocol in adult mice following nNOS blockade protocol at P5–7 (top). Bottom: FOR- (C) and cFC (D)-recall and cFos+/Lsi1/2 cells in vCA3b (saline control and L-NAME treated mice). cFC recall in training and neutral (N) context (D). Black circles: values from individual mice. Ordinary two-way ANOVA followed by Sidak's multiple comparison post-hoc test (A). Ordinary one-way ANOVA followed by Kruskal-Wallis's multiple comparison post-hoc test (B). Unpaired Student's t test (C) and (D), FOR/cFC memory. Ordinary two-way ANOVA followed by Fischer's multiple comparison post-hoc test (C) and (D), cFos in Lsi1 and Lsi2 cells. $p < 0.05$ (*), $p < 0.01$ (**), $p < 0.001$ (***), and $p < 0.0001$ (****). $n = 3–4$ (A), $n = 3–4$ (B), and $n = 3–9$ (C) and (D).

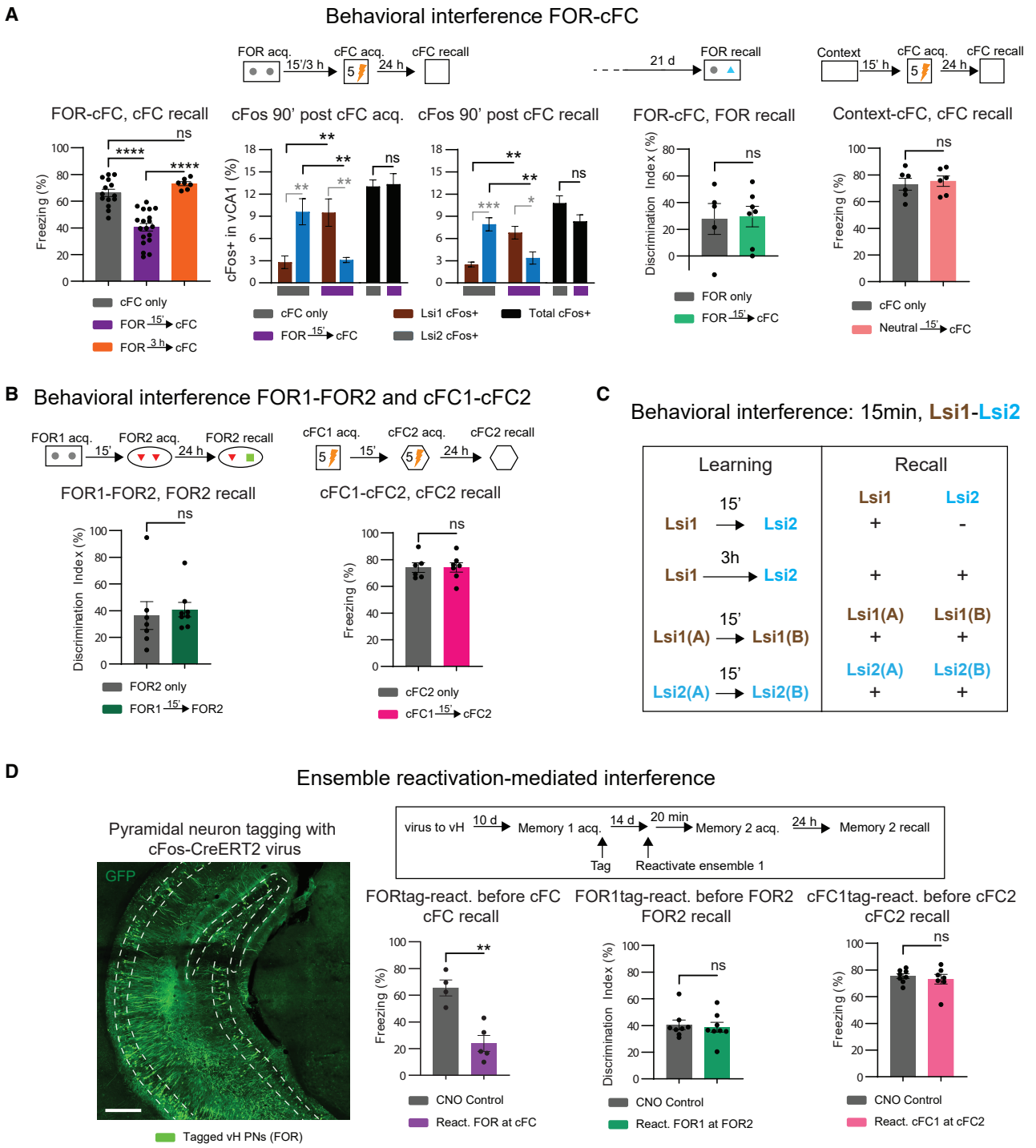

Figure 6. Lsi-type exclusive memory formation time window: behavioral and ensemble activation evidence

(A) Interference by acquisition of FOR on subsequent acquisition of cFC. Left: impact on cFC recall and on cFos expression in Lsi1 and Lsi2 PNs 90 min after acquisition or 90 min after recall; center: impact on FOR recall; right: comparison to novel context without objects, instead of FOR-cFC.

(B) No interference between acquisition of FOR1 and FOR2 (left) and cFC1and cFC2 (right), respectively.

(C) Lsi2-type learning specifically prevented when occurring 15 min subsequent to learning involving allocation to Lsi1 PNs; detection at recall.

(legend continued on next page)

P5–7 or P7–9: clusters of Lsi2 LMTs onto Lsi2 CA3b PNs were less tight in P5–7 treated mice, but no extra clusters were induced by Lsi2 mossy fibers onto non-Lsi2 CA3b PNs (Figure 5B). These results are consistent with our previous findings that selective synaptogenesis within hippocampal Lsi1 and Lsi2 neurons is mainly based on a temporal competence mechanism, meaning that when synaptogenesis by Lsi1 neurons is delayed, it can then also occur with temporally competent Lsi2 neurons, leading to a disruption of Lsi1/2 specificity.[36]

We then carried out FOR (Lsi1-type learning) and cFC (Lsi2-type learning) experiments in adult Lsi1 and Lsi2 mice treated with L-NAME during the P5–7 time window. Consistent with the notion that cFos expression in Lsi1 neurons might be critically important for memory in FOR, mice treated with L-NAME at P5–7 failed to exhibit the expected cFos expression in Lsi1 neurons and exhibited a complete disruption of memory at recall of FOR (Figure 5C). Unlike upon Syt2+PV+ inhibition 15 min after acquisition, loss of cFos expression in Lsi1 neurons upon FOR was not accompanied by expression of cFos in Lsi2 neurons in P5–7 L-NAME treated mice (Figure 5C). Furthermore, upon cFC, P5–7 L-NAME-treated mice exhibited robust abnormal induction of cFos expression in Lsi1 neurons, with no corresponding reduction in the induction of cFos in Lsi2 neurons (Figure 5D). Consistent with the notion that cFos expression in Lsi2 neurons is critically important for memory upon cFC, L-NAME-treated mice only exhibited a modest reduction in freezing upon cFC at recall (from 80% to about 58% of time compared to about 15% of time upon inhibition of vH and dH [about 40% of time upon inhibition of vH]; Figure 5D). In parallel, and notably, L-NAME-treated mice with abnormal induction of cFos expression in Lsi1 neurons upon cFC exhibited a dramatic increase in freezing in a neutral context (from about 4% in untreated mice to 40% in L-NAME P5–7 mice; Figure 5D). When combined with those of the Syt2+PV+ inhibition experiments, these results provided evidence that cFos expression in the appropriate subpopulation of PNs (Lsi1 for FOR and Lsi2 for cFC) is critically important for memory formation. Furthermore, by showing that loss of cFos expression in one subpopulation does not by itself lead to expression in the opposite Lsi subpopulation, these results further suggested that learning-related allocation to the opposite Lsi1/2 subpopulation upon cFC or FOR is a specific consequence of Syt2+PV+ neuron inhibition during a critical time window for memory formation upon learning.

Lsi-type exclusive memory formation time window: Behavioral evidence

We next investigated whether memory allocation to one particular hippocampal Lsi network during its Syt2+ time window might interfere with initiation of memory allocation processes involving the opposite Lsi subpopulation (Figure 6A). When acquisition of FOR, a task depending on vH, preceded by 15 min acquisition of subsequent cFC, fear memory, as tested at recall 24 h later, was reduced to an extent comparable to when vH Syt2+ neurons were inhibited 15 min after cFC acquisition (Figure 6A). Notably, when FOR preceded cFC by 15 min, we did not detect any induction of cFos expression in Lsi2 neurons (in addition to FOR-related Lsi1 neurons) 90 min after acquisition or at recall (Figure 6A). No interference with fear memory was detected when FOR preceded cFC acquisition by 3 h (Figure 6A). Furthermore, when mice were exposed 15 min before the cFC protocol to a novel context in the absence of novel objects to engage with, fear memory formation was unaffected (Figure 6A). Notably, while FOR acquisition interfered with subsequent cFC acquisition in the FOR-cFC protocol, subsequent cFC acquisition 15 min after FOR did not interfere with FOR memory (Figure 6A), indicating that in these experiments, behavioral interference selectively involves subsequent learning occurring within the memory formation time window.

To investigate the notion that interference specifically occurs when the first learning process involves cFos allocation to the Lsi network opposite to that of the second learning process, we carried out sequential FOR-FOR and cFC-cFC learning protocols (Figure 6B). When two FOR acquisition protocols (FOR1 and FOR2) carried out in two different contexts and with different objects were separated by 15 min, no interference by FOR1 was detected on memory formation in FOR2 (Figure 6B). Likewise, when cFC1 preceded cFC2 (different contexts) by 15 min, no interference with memory formation in cFC2 was detected at recall on the subsequent day (Figure 6B). Therefore, learning is specifically prevented when it is preceded, 15 min but not 3 h before, by a learning protocol involving selective cFos+ neuron allocation to the opposite Lsi subpopulation (Figure 6C).

Lsi-type exclusive memory formation time window: Ensemble activation evidence

To further probe the notion that selective recruitment of a particular cFos+ subpopulation of Lsi neurons interferes with learning involving the opposite Lsi subpopulation within the time window for Syt2+-dependent memory formation, we carried out cFos+ memory ensemble tagging (Figures 6D and S5G) and reactivation experiments, followed by learning involving opposite or same Lsi subpopulation recruitment. cFos+ neurons were tagged through tamoxifen and Cre-dependent DREADDs activator delivery 30 min after acquisition of FOR or cFC using a *TRAP2-CreERT2* virus strategy[48,53] in which Tamoxifen-dependent Cre expression is directed from the cFos locus (*cFos-CreERT2* virus) and tagged neurons were reactivated with DREADDs ligand CNO 20 min before a new learning protocol (Figures 6D and S5G). Control experiments provided evidence that the tagging process with virus was efficient and specific. Thus, neurons tagged at acquisition (virus or TRAP2 mice) exhibited robust overlap with cFos-expressing neurons at recall of cFC or FOR, whereas the overlap with neurons tagged and "recalled" in the home cage was very low (Figure S5G).

(D) Left: representative image of tagged vH cFos-expressing neurons (GFP+) upon FOR (analysis 14 days after FOR). Right: interference by FOR memory ensemble reactivation on subsequent acquisition of cFC. Scale bars, 100 μm. Ordinary one-way ANOVA followed by Tukey's multiple comparison post-hoc test (A), left plot, behavioral readout; $p < 0.0001$ and $F = 34.23$. $p < 0.0001$ (****). Ordinary two-way ANOVA followed by Fisher's least significant difference multiple comparison post-hoc test (A, left plot, cFos expression in Lsi1/2 PNs); $p < 0.05$ (*), $p < 0.01$ (**), and $p < 0.001$ (***). Unpaired Student's t test (A), middle and right plots (B) and (D); $p < 0.01$ (**). $n = 4–19$ (A), 7–8 (B), and 4–8 (D). See also Figure S5.

Activation of FOR ensembles (Lsi1 learning) before acquisition of cFC (Lsi2 learning) produced greatly diminished fear memory at 24 h recall (Figure 6D). By contrast, activation of a cFC1 ensemble 20 min before acquisition of cFC2 did not interfere with cFC2 memory formation as tested at recall (Figure 6D). Likewise, activation of a FOR1 ensemble 20 min before acquisition of FOR2 learning did not interfere with recall of FOR2 (Figure 6D). Therefore, and consistent with the notion that in these experiments, interference involves attempted allocation to memory ensembles of opposite Lsi-type within the Syt2+ time window for memory allocation, cFos+ ensemble activation before a learning protocol of opposite Lsi-type specifically prevents memory formation.

DISCUSSION

Our study uncovers an early time window for memory formation, specifically depending on the activity of local early-born Syt2+, but not late-born Syt2−PV+ neurons. Stable allocation of the correct subpopulation of PNs to the newly forming memory ensemble specifically depended on Syt2+PV+ neuron activity during the early time window for memory formation. Distinct PN subpopulations were allocated to hippocampal memory ensembles upon FOR (Lsi1) or cFC (Lsi2), and failure to do so was associated with memory failure. Interference experiments involving sequential recruitment of the Lsi1 and Lsi2 PNs within the early time window for memory formation revealed that early time window recruitment of one subpopulation of PNs prevented memory formation for a second learning process when the latter involved recruitment of the opposite subpopulation. Taken together, our results reveal that memory ensemble allocation to the proper subpopulation of PNs upon learning is a critical early step in memory formation, specifically depending on the activity of Syt2+ ePV neurons.

An early time window for memory formation after learning

Our results have uncovered a critical early formation time window in the long-term memory formation-consolidation process defined by a specific dependence on the activity of early-born Syt2+PV+ but not late-born Syt2−PV+ neurons. This early time window was followed by memory consolidation time windows and retrieval processes, specifically depending on the activity of Syt2− but not Syt2+ PV neurons. Given the well-established role of PV-expressing interneurons in supporting and shaping network dynamics,[4,12,54] the striking switch from dependence on the activity of Syt2+PV+ neurons to that of Syt2−PV+ neurons suggests that the end of the early time window for memory formation might coincide with a shift in the ensemble's dependence on learning-related network dynamics.

The timing of the Syt2+-dependent early time window coincides with the appearance of early plasticity markers such as phosphorylation of signal transduction mediators, including the MAP kinase pERK and the cAMP mediator CREB, indiscriminately in Lsi1 and Lsi2 PNs. By contrast, detectable translation of immediate-early genes, such as *Arc* and *cFos*, critically important for plasticity and memory consolidation, occurs subsequent to closing of the Syt2+-dependent time window. Interestingly, like pERK and pCREB (15 min after acquisition), Arc was not expressed selectively in the proper subpopulation of PNs 30 min after acquisition. By contrast, Arc expression at 60 min and learning-related cFos protein expression, first prominent at 45 min, were specifically detected in the proper PN subpopulation. These results suggest that specific allocation-mediating processes during the early Syt2+-dependent time window for memory formation have critical roles in predetermining subsequent long-term plasticity and memory processes in the appropriate PN subpopulations. While the actual processes and mechanisms remain to be determined, one scenario consistent with the dynamics of plasticity marker expression upon learning is that Syt2+ PV+-dependent network activity processes are enhanced, reducing the critical permissive cellular plasticity processes in Lsi1/2 PNs preselected at the time of acquisition.

Early memory formation time window involves allocation to proper Lsi1/2 PN subpopulation

Our results suggest that online network activity involved in learning, and likely involving large fractions of local neurons is followed by a distinct early phase of offline network activity, critical for allocating fractions of learning-related neurons to newly forming ensembles important for consolidation and subsequent retrieval of memory.[9] Our results could be reconciled with a model in which the type of learning might select the proper Lsi subpopulation at acquisition, prior to Syt2+PV+-dependent allocation of memory-related plasticity processes to the specific subpopulation of PNs.

The results of our behavioral interference and ensemble activation experiments provide evidence that conditions promoting ensemble allocation to neurons belonging to a particular PN subpopulation during the early time window for memory formation interfere with the formation of subsequent memories involving different PN subpopulations. In potentially related interference experiments, engram activation was necessary for behavioral interference of memory,[55] and increased cortical plasticity could promote memory interference.[56] Our results suggest that at any given time, local networks influenced by Syt2+PV+ neurons can either support Lsi1- or Lsi2-type PN subpopulation recruitment to memory ensembles. As mentioned earlier, these findings would be consistent with a model in which activity in Syt2+PV+ neurons during the 15-min time window enhances allocation-promoting plasticity processes in the proper Lsi PN subpopulation while depressing corresponding processes in the opposite Lsi subpopulation. While the basis for the striking Lsi1/2 dichotomy remains to be determined, a possible interpretation consistent with previous findings on hippocampal subpopulations[38] is that parallel, largely non-overlapping circuits involving Lsi1- or Lsi2-type PNs might represent functionally distinct modules engaged in distinct types of learning. Consistent with this interpretation, the results of our experiments involving Syt2+ PV+ inhibition as well as L-NAME treatment at P5–7 indicate that memory formation fails whenever cFos is not induced in the proper Lsi subpopulation, whereas cFos expression in the wrong subpopulation only modifies learning-related memory if occurring in addition to the proper subpopulation (L-NAME and cFC). Interestingly, broader PN subpopulation groups involving early-born PNs (which possibly include the Lsi1/2 subpopulations)

and late-born PNs have further specific roles during different phases of memory consolidation and retrieval,[57] suggesting the involvement of a complex repertoire of partially overlapping PN subpopulations in memory formation and consolidation processes.

Syt2+ neuron dependence for allocation time window

We found that memory formation and recall were prevented when all PV+ neurons are inhibited at any time during the first 5 h after acquisition, during a 12-h late memory consolidation time window or upon recall. By contrast, just inhibiting early born Syt2+PV+ neurons specifically prevented memory formation during the early time window, whereas activity in late-born Syt2−PV+ neurons specifically accounted for memory formation and recall at any other time. ePV neurons exhibit substantially higher densities of excitatory boutons onto their somas and proximal dendrites than their late-born counterparts, and their plasticity is specifically influenced by changes in excitation.[39] Furthermore, and notably, the expression of Syt2 is critically important for effective transmitter release in fast-spiking neurons.[58–65] Accordingly, although how Syt2+PV+ neuron physiology and connectivity relate to their unique role in memory formation remains to be determined, the available evidence is consistent with critical roles in high-frequency oscillatory network modulation, possibly driven by strong excitatory inputs onto early-born Syt2+PV+ neurons during neuronal allocation to the forming memory ensemble early after acquisition.

Conclusions and outlook

Our results establish allocation of the proper subpopulation of PNs to the newly assembling memory ensemble as a critical early step in the memory formation process, specifically depending on activity in early-born Syt2+PV+ interneurons during an early time window after acquisition. The transition from early Syt2+PV+ neuron-dependent memory allocation to subsequent Syt2−PV+ neuron-dependent memory consolidation and retrieval suggests a scenario in which early memory allocation processes involving oscillatory network activity, depending on early-born Syt2+PV+ neurons, might run in parallel to longer-lasting memory consolidation and retrieval processes within local networks. Our findings uncovering distinct roles of PV neuron subpopulations for local network activity processes suggest that partly overlapping local networks of PNs and inhibitory interneurons might account for distinct activity-dependent processes co-existing at any time within local and distributed networks.[35,66] How such parallel network dynamics processes might interface with corresponding plasticity processes and neuronal connectivity schemes remains to be determined.

Limitations of the study

Our study identifies an early time window for proper memory ensemble allocation and memory formation after learning, specifically depending on activity in early-born Syt2+PV+ interneurons, but it does not address electrophysiological and/or connectivity features that might be specific to PV interneuron subpopulations and might influence their specific roles in memory.

RESOURCE AVAILABILITY

Lead contact

Further information and requests for resources and reagents should be directed to and will be fulfilled by the lead contact, Pico Caroni (caroni@fmi.ch).

Materials availability

All unique/stable reagents generated in this study are available from the lead contact with a completed materials transfer agreement.

Data and code availability

- All data, including microscopy data reported in the paper, will be shared by the lead contact upon request.
- The custom code has been deposited in GitHub repository (https://github.com.bhankoma/Valbuena-et-al-2025.git) and at Zenodo (https://doi.org/10.5281/zenodo.15878942) and is publicly available as of the date of publication. DOI is stated in the key resources table.
- Any additional information required to reanalyze the data reported in this work paper is available from the lead contact upon request.

ACKNOWLEDGMENTS

We thank members of the Caroni group for discussions about the project. We thank Maria Lahr (FMI) for contributing some of the data regarding the role of dH and vH in extinction learning. We thank Silvia Arber (University of Basel) for valuable comments on the manuscript. Harsh Kanodia (Univ. of Basel) helped with the LFP experiments and their surgeries. S.V. was supported by a long-term fellowship from EMBO. A.U., M.T., and K.B. were supported by the Novartis Research Foundation (FMI).

AUTHOR CONTRIBUTIONS

S.V. and P.C. devised the study. S.V. and K.B. conducted experiments and analyses involving subpopulation inhibition and behavior, electrophysiological recordings, and cFos analysis. A.U. conducted experiments on unperturbed Lsi1 and Lsi2 cFos expression upon behavior and on the role of nNOS during synaptogenesis on Lsi1/2 selective connectivity and learning. M.T. carried out the identification of PV subpopulation markers as well as the development of *Syt2-Cre* mice. P.C. wrote the manuscript.

DECLARATION OF INTERESTS

The authors declare no competing interests.

STAR★METHODS

Detailed methods are provided in the online version of this paper and include the following:

- KEY RESOURCES TABLE
- EXPERIMENTAL MODEL AND SUBJECT DETAILS
  - Mice
- METHOD DETAILS
  - Retrovirus production and purification
  - *In utero* injections
  - Acute brain slice and single cell collection for Smart-seq
  - Stereotaxic surgery
  - Behavior
  - Memory ensemble tagging and reactivation
  - Trap2 virus and controls
  - Optogenetic inhibition of $Syt2^{+}PV^{+}$ neurons
  - Interference with Lsi PN synaptogenesis in hippocampal vCA3
  - Connectivity analyses in nNOS inhibition experiments
  - *In vivo* electrophysiology
  - Immunohistochemistry
  - Birthdating experiments
- QUANTIFICATION AND STATISTICAL ANALYSIS

SUPPLEMENTAL INFORMATION

Supplemental information can be found online at https://doi.org/10.1016/j.celrep.2025.116144.

Received: December 2, 2024
Revised: January 28, 2025
Accepted: July 22, 2025

REFERENCES

1. Zhou, Y., Won, J., Karlsson, M.G., Zhou, M., Rogerson, T., Balaji, J., Neve, R., Poirazi, P., and Silva, A.J. (2009). CREB regulates excitability and the allocation of memory to subsets of neurons in the amygdala. Nat. Neurosci. *12*, 1438–1443. https://doi.org/10.1038/nn.2405.
2. Han, J.H., Kushner, S.A., Yiu, A.P., Hsiang, H.L.L., Buch, T., Waisman, A., Bontempi, B., Neve, R.L., Frankland, P.W., and Josselyn, S.A. (2009). Selective erasure of a fear memory. Science *323*, 1492–1496. https://doi.org/10.1126/science.1164139.
3. Josselyn, S.A., and Tonegawa, S. (2020). Memory engrams: Recalling the past and imagining the future. Science *367*, eaaw4325. https://doi.org/10.1126/science.aaw4325.
4. Buzsaki, G., McKenzie, S., and Davachi, L. (2022). Neurophysiology of remembering. Ann. Rev. Psychol. *73*, 187–215. https://doi.org/10.1146/annurev-psych-021721-110002.
5. Yuste, R., Cossart, R., and Yaksi, E. (2024). Neuronal ensembles: Building blocks of neural circuits. Neuron *112*, 875–892. https://doi.org/10.1016/j.neuron.2023.12.008.
6. Fernandez-Ruiz, A., Oliva, A., Fermino de Oliveira, E., Rocha-Almeida, F., Tingley, D., and Buzsaki, G. (2019). Long-duration hippocampal sharp wave ripples improve memory. Science *364*, 1082–1086. https://doi.org/10.1126/science.aax0758.
7. Terada, S., Geiller, T., Liao, Z., O'Hare, J., Vancura, B., and Losonczy, A. (2022). Adaptive stimulus selection for consolidation in the hippocampus. Nature *601*, 240–244. https://doi.org/10.1038/s41586-021-04118-6.
8. Zaki, Y., and Cai, D.J. (2024). Memory engram stability and flexibility. Neurpsychopharmacology *50*, 285–293. https://doi.org/10.1038/s41386-024-01979-z.
9. Yang, W., Sun, C., Huszár, R., Hainmueller, T., Kiselev, K., and Buzsáki, G. (2024). Selection of experience for memory by hippocampal sharp wave ripples. Science *383*, 1478–1483. https://doi.org/10.1126/science.adk8261.
10. Feng, F., Samarth, P., Paré, D., and Nair, S.S. (2016). Mechanisms underlying the formation of the amygdalar fear memory trace: A computational perspective. Neuroscience *322*, 370–376. https://doi.org/10.1016/j.neuroscience.2016.02.059.
11. Topolnik, L., and Tamboli, S. (2022). The role of inhibitory circuits in hippocampal memory processing. Nat. Rev. Neurosci. *23*, 476–492. https://doi.org/10.1038/s41583-022-00599-0.
12. Tukker, J.J., Lasztóczi, B., Katona, L., Roberts, J.D.B., Pissadaki, E.K., Dalezios, Y., Márton, L., Zhang, L., Klausberger, T., and Somogyi, P. (2013). Distinct dendritic arborization and in vivo firing patterns of parvalbumin-expressing basket cells in the hippocampal area CA3. J. Neurosci. *33*, 6809–6825. https://doi.org/10.1523/JNEUROSCI.5052-12.2013.
13. Hu, H., Gan, J., and Jonas, P. (2014). Interneurons. Fast-spiking, parvalbumin(+) GABAergic interneurons: from cellular design to microcircuit function. Science *345*, 1255263. https://doi.org/10.1126/science.1255263.
14. Drew, L.J., Kheirbek, M.A., Luna, V.M., Denny, C.A., Cloidt, M.A., Wu, M.V., Jain, S., Scharfman, H.E., and Hen, R. (2016). Activation of local inhibitory circuits in the dentate gyrus by adult-born neurons. Hippocampus *26*, 763–778. https://doi.org/10.1002/hipo.22557.
15. Rashid, A.J., Yan, C., Mercaldo, V., Hsiang, H.L.L., Park, S., Cole, C.J., De Cristofaro, A., Yu, J., Ramakrishnan, C., Lee, S.Y., et al. (2016). Competition between engrams influences fear memory formation and recall. Science *353*, 383–387. https://doi.org/10.1126/science.aaf0594.
16. Morrison, D.J., Rashid, A.J., Yiu, A.P., Yan, C., Frankland, P.W., and Josselyn, S.A. (2016). Parvalbumin interneurons constrain the size of the lateral amygdala engram. Neurobiol. Learn. Mem. *135*, 91–99. https://doi.org/10.1016/j.nlm.2016.07.007.
17. Agetsuma, M., Hamm, J.P., Tao, K., Fujisawa, S., and Yuste, R. (2018). Parvalbumin-Positive Interneurons Regulate Neuronal Ensembles in Visual Cortex. Cereb. Cortex *28*, 1831–1845. https://doi.org/10.1093/cercor/bhx169.
18. Trifilieff, P., Herry, C., Vanhoutte, P., Caboche, J., Desmedt, A., Riedel, G., Mons, N., and Micheau, J. (2006). Foreground contextual fear memory consolidation requires two independent phases of hippocampal ERK/CREB activation. Learn. Mem. *13*, 349–358. https://doi.org/10.1101/lm.80206.
19. Holtmaat, A., and Caroni, P. (2016). Functional and structural underpinnings of neuronal assembly formation in learning. Nat. Neurosci. *19*, 1553–1562. https://doi.org/10.1038/nn.4418.
20. Karunakaran, S., Chowdhury, A., Donato, F., Quairiaux, C., Michel, C.M., and Caroni, P. (2016). PV plasticity sustained through D1/5 dopamine signaling required for long-term memory consolidation. Nat. Neurosci. *19*, 454–464. https://doi.org/10.1038/nn.4231.
21. Chowdhury, A., and Caroni, P. (2018). Time units for learning involving maintenance of system-wide cFos expression in neuronal assemblies. Nat. Commun. *9*, 4122. https://doi.org/10.1038/s41467-018-06516-3.
22. Han, J.H., Kushner, S.A., Yiu, A.P., Cole, C.J., Matynia, A., Brown, R.A., Neve, R.L., Guzowski, J.F., Silva, A.J., and Josselyn, S.A. (2007). Neuronal competition and selection during memory formation. Science *316*, 457–460. https://doi.org/10.1126/science.1139438.
23. Flavell, S.W., and Greenberg, M.E. (2008). Signaling mechanisms linking neuronal activity to gene expression and plasticity of the nervous system. Annu. Rev. Neurosci. *31*, 563–590. https://doi.org/10.1146/annrev.neuro.31.060407.
24. Kim, D., Paré, D., and Nair, S.S. (2013). Assignment of model amygdala neurons to the fear memory trace depends on competitive synaptic interactions. J. Neurosci. *33*, 14354–14358. https://doi.org/10.1523/JNEUROSCI.2430-13.2013.
25. Yiu, A.P., Mercaldo, V., Yan, C., Richards, B., Rashid, A.J., Hsiang, H.L.L., Pressey, J., Mahadevan, V., Tran, M.M., Kushner, S.A., et al. (2014). Neurons are recruited to a memory trace based on relative neuronal excitability immediately before training. Neuron *83*, 722–735. https://doi.org/10.1016/j.neuron.2014.07.017.
26. Park, S., Kramer, E.E., Mercaldo, V., Rashid, A.J., Insel, N.,, Frankland, P.W., and Josselyn, S.A. (2016). Neuronal Allocation to a Hippocampal Engram. Neuropsychopharmacology *41*, 2987–2993. https://doi.org/10.1038/npp.2016.73.
27. Josselyn, S.A., and Frankland, P.W. (2018). Memory Allocation: Mechanisms and Function. Annu. Rev. Neurosci. *41*, 389–413. https://doi.org/10.1146/annurev-neuro-080317-061956.
28. Rao-Ruiz, P., Yu, J., Kushner, S.A., and Josselyn, S.A. (2019). Neuronal competition: microcircuit mechanisms define the sparsity of the engram. Curr. Opin. Neurobiol. *54*, 163–170. https://doi.org/10.1016/j.conb.2018.10.013.
29. Pignatelli, M., Ryan, T.J., Roy, D.S., Lovett, C., Smith, L.M., Muralidhar, S., and Tonegawa, S. (2019). Engram cell excitability state determines the efficacy of memory retrieval. Neuron *101*, 274–284.e5. https://doi.org/10.1016/j.neuron.2018.11.029.
30. Gulmez Karaca, K., Kupke, J., and Oliveira, A.M.M. (2021). Molecular and cellular mechanisms of engram allocation and maintenance. Brain Res. Bull. *170*, 274–282. https://doi.org/10.1016/j.brainresbull.2021.02.019.

31. Delamare, G., Zaki, Y., Cai, D.J., and Clopath, C. (2024). Drift of neural ensembles driven by slow fluctuations of intrinsic excitability. eLife *12*, R88053. https://doi.org/10.7554/eLife.88053.

32. Luis, C.O.d.S., Pezzoli, M., Urrieta, E., and Ryan, T.J. (2023). Engram cell connectivity as a mechanism for information encoding and memory function. Preprint at bioRxiv. https://doi.org/10.1101/2023.09.21.558774.

33. Delamare, G., Tomé, D.F., and Clopath, C. (2024). Intrinsic neural excitability biases allocation and overlap of memory engrams. J. Neurosci. *44*, e0846232024. https://doi.org/10.1523/JNEUROSCI.0846-23.2024.

34. Hansel, C., and Yuste, R. (2024). Neural ensembles: role of intrinsic excitability and its plasticity. Front. Cell. Neurosci. *18*, 1440588. https://doi.org/10.3389/fncel.2024.1440588.

35. Zheng, Z.S., Huszár, R., Hainmueller, T., Bartos, M., Williams, A.H., and Buzsáki, G. (2024). Perpetual step-like restructuring of hippocampal circuit dynamics. Cell Rep. *43*, 114702. https://doi.org/10.1101/2024.04.22.590576.

36. Deguchi, Y., Donato, F., Galimberti, I., Cabuy, E., and Caroni, P. (2011). Temporally matched subpopulations of selectively interconnected principal neurons in the hippocampus. Nat. Neurosci. *14*, 495–504. https://doi.org/10.1038/nn.2768.

37. Druckmann, S., Feng, L., Lee, B., Yook, C., Zhao, T., Magee, J.C., and Kim, J. (2014). Structured synaptic connectivity between hippocampal regions. Neuron *81*, 629–640. https://doi.org/10.1016/j.neuron.2013.11.026.

38. Huszar, R., Zhang, Y., Blockus, H., and Buzsaki, G. (2022). Preconfigured dynamics in the hippocampus are guided by embryonic birthdate and rate of neurogenesis. Nat. Neurosci. *25*, 1201–1212. https://doi.org/10.1038/s41593-022-01138-x.

39. Donato, F., Chowdhury, A., Lahr, M., and Caroni, P. (2015). Early- and late-born parvalbumin basket cell subpopulations exhibiting distinct regulation and roles in learning. Neuron *85*, 770–786. https://doi.org/10.1016/j.neuron.2015.01.011.

40. Donato, F., Rompani, S.B., and Caroni, P. (2013). Parvalbumin-expressing basket-cell network plasticity induced by experience regulates adult learning. Nature *504*, 272–276. https://doi.org/10.1038/nature12866.

41. Tashiro, A., Zhao, C., and Gage, F.H. (2006). Retrovirus-mediated single-cell gene knockout technique in adult newborn neurons in vivo. Nat. Protoc. *1*, 3049–3055. https://doi.org/10.1038/nprot.2006.473.

42. Picelli, S., Faridani, O.R., Björklund, A.K., Winberg, G., Sagasser, S., and Sandberg, R. (2014). Full-length RNA-seq from single cells using Smart-seq2. Nat. Protocols *9*, 171–181. https://doi.org/10.1038/nprot.2014.006.

43. Fenno, L.E., Mattis, J., Ramakrishnan, C., Hyun, M., Lee, S.Y., He, M., Tucciarone, J., Selimbeyoglu, A., Berndt, A., Grosenick, L., et al. (2014). Targeting cells with single vectors using multiple-feature Boolean logic. Nat. Methods *11*, 763–772. https://doi.org/10.1038/nmeth.2996.

44. Madisen, L., Garner, A.R., Shimaoka, D., Chuong, A.S., Klapoetke, N.C., Li, L., van der Bourg, A., Niino, Y., Egolf, L., Monetti, C., et al. (2015). Transgenic mice for intersectional targeting of neural sensors and effectors with high specificity and performance. Neuron *85*, 942–958. https://doi.org/10.1016/j.neuron.2015.02.022.

45. Sternson, S.M., and Roth, B.L. (2014). Chemogenetic tools to interrogate brain functions. Annu. Rev. Neurosci. *37*, 387–407. https://doi.org/10.1146/annurev-neuro-071013-014048.

46. Atasoy, D., and Sternson, S.M. (2018). Chemogenetic tools for causal cellular and neuronal biology. Physiol. Rev. *98*, 391–418. https://doi.org/10.1152/physrev.00009.2017.

47. Serrano, M., Tripodi, M., and Caroni, P. (2022). Strategy updating mediated by specific retrosplenial-parafascicular-basal ganglia networks. Curr. Biol. *32*, 3477–3492.e5. https://doi.org/10.1016/j.cub.2022.06.033.

48. Bhandari, K., Kanodia, H., Donato, F., and Caroni, P. (2024). Selective vulnerability of the ventral hippocampus-prelimbic cortex axis parvalbumin interneuron network underlies learning deficits of fragile X mice. Cell Rep. *43*, 114124. https://doi.org/10.1016/j.celrep.2024.114124.

49. Lemke, S.M., Ramanathan, D.S., Guo, L., Won, S.J., and Ganguly, K. (2019). Emergent modular neural control drives coordinated motor actions. Nat. Neurosci. *22*, 1122–1131. https://doi.org/10.1038/s41593-019-0407-2.

50. Petersen, P.C., Siegle, J.H., Steinmetz, N.A., Mahallati, S., and Buzsáki, G. (2021). CellExplorer: A framework for visualizing and characterizing single neurons. Neuron *109*, 3594–3608.e2. https://doi.org/10.1016/j.neuron.2021.09.002.

51. Ogilvie, P., Schiling, K., Billinsley, M.L., and Schmidt, H.H.W. (1995). Induction and variants of neuronal nitric oxide synthase type 1 during synpatogenesis. FASEB J. *9*, 799–806. https://doi.org/10.1096/fasebj.9.9.7541381.

52. Nikonenko, I., Boda, B., Steen, S., Knott, G., Welker, E., and Muller, D. (2008). PSD-95 promotes synaptogenesis and multiinnervated spine formation through nitric oxide signaling. J. Cell Biol. *183*, 1115–1127. https://doi.org/10.1083/jcb.200805132.

53. DeNardo, L.A., Liu, C.D., Allen, W.E., Adams, E.L., Friedmann, D., Fu, L., Guenthner, C.J., Tessier-Lavigne, M., and Luo, L. (2019). Temporal evolution of cortical ensembles promoting remote memory retrieval. Nat. Neurosci. *22*, 460–469. https://doi.org/10.1038/s41593-018-0318-7.

54. Huang, Y.-C., Chen, H.-C., Lin, Y.-T., Lin, S.-T., Zheng, Q., Abdelfattah, A. S., Lavis, L.D., Schreiter, E.R., Lin, B.-J., and Chen, T.-W. (2024). Dynamic assemblies of parvalbumin interneurons in brain oscillations. Neuron *112*, 2600–2613.e5. https://doi.org/10.1016/j.neuron.2024.05.015.

55. Autore, L., O'Leary, J.D., Ortega-de San Luis, C., and Ryan, T.J. (2023). Adaptive expression of engrams by retroactive interference. Cell Rep. *42*, 112999. https://doi.org/10.1016/j.celrep.2023.112999.

56. Navarro Lobato, I., Aleman-Zapata, A., Samanta, A., Bogers, M., Narayanan, S., Rayan, A., Alonso, A., van der Meij, J., Khamassi, M., Khan, Z.U., and Genzel, L. (2023). Increased cortical plasticity leads to memory interference and enhanced hippocampal-cortical interactions. eLife *12*, e84911. https://doi.org/10.7554/eLife.84911.

57. Kveim, V.A., Salm, L., Ulmer, T., Lahr, M., Kandler, S., Imhof, F., and Donato, F. (2024). Divergent recruitment of developmentally defined neuronal ensembles supports memory dynamics. Science *385*, eakd0997. https://doi.org/10.1126/science.adk0997.

58. Pang, Z.P., Melicoff, E., Padgett, D., Liu, Y., Teich, A.F., Dickey, B.F., Lin, W., Adachi, R., and Südhof, T.C. (2006). Synaptotagmin-2 is essential for survival and contributes to Ca2+ triggering of neurotransmitter release in central and neuromuscular synapses. J. Neurosci. *26*, 13493–13504. https://doi.org/10.1523/JNEUROSCI.3519-06.2006.

59. Xu, J., Mashimo, T., and Südhof, T.C. (2007). Synaptotagmin-1, -2, and -9: Ca(2+) sensors for fast release that specify distinct presynaptic properties in subsets of neurons. Neuron *54*, 567–581. https://doi.org/10.1016/j.neuron.2007.05.004.

60. Kerr, A.M., Reisinger, E., and Jonas, P. (2008). Differential dependence of phasic transmitter release on synaptotagmin 1 at GABAergic and glutamatergic hippocampal synapses. Proc. Natl. Acad. Sci. USA *105*, 15581–15586. https://doi.org/10.1073/pnas.0800621105.

61. Sommeijer, J.P., and Levelt, C.N. (2012). Synaptotagmin-2 is a reliable marker for parvalbumin positive inhibitory boutons in the mouse visual cortex. PLoS One *7*, e35323. https://doi.org/10.1371/journal.pone.0035323.

62. Paul, A., Crow, M., Raudales, R., He, M., Gillis, J., and Huang, Z.J. (2017). Transcriptional Architecture of Synaptic Communication Delineates GABAergic Neuron Identity. Cell *171*, 522–539.e20. https://doi.org/10.1016/j.cell.2017.08.032.

63. Chen, C., Arai, I., Satterfield, R., Young, S.M., Jr., and Jonas, P. (2017). Synaptotagmin 2 Is the Fast Ca(2+) Sensor at a Central Inhibitory Synapse. Cell Rep. *18*, 723–736. https://doi.org/10.1016/j.celrep.2016.12.067.

64. Harris, K.D., Hochgerner, H., Skene, N.G., Magno, L., Katona, L., Bengtsson Gonzales, C., Somogyi, P., Kessaris, N., Linnarsson, S., and Hjerling-Leffler, J. (2018). Classes and continua of hippocampal CA1 inhibitory

neurons revealed by single-cell transcriptomics. PLoS Biol. *16*, e2006387. https://doi.org/10.1371/journal.pbio.2006387.

65. Favuzzi, E., Deogracias, R., Marques-Smith, A., Maeso, P., Jezequel, J., Exposito-Alonso, D., Balia, M., Kroon, T., Hinojosa, A.J., F Maraver, E., and Rico, B. (2019). Distinct molecular programs regulate synapse specificity in cortical inhibitory circuits. Science *363*, 413–417. https://doi.org/10.1126/science.aau8977.

66. Garcia-Junco-Clemente, P., Tring, E., Ringach, D.L., and Trachtenberg, J. T. (2019). State-Dependent Subnetworks of Parvalbumin-Expressing Interneurons in Neocortex. Cell Rep. *26*, 2282–2288.e3. https://doi.org/10.1016/j.celrep.2019.02.005.

67. Zhang, Z., Ferretti, V., Güntan, I., Moro, A., Steinberg, E.A., Ye, Z., Zecharia, A.Y., Yu, X., Vyssotski, A.L., Brickley, S.G., et al. (2015). Neuronal ensembles sufficient for recovery sleep and the sedative actions of a2 adrenergic agonists. Nat. Neurosci. *18*, 553–561. https://doi.org/10.1038/nn.3957.

68. Guenthner, C.J., Miyamichi, K., Yang, H.H., Heller, H.C., and Luo, L. (2013). Permanent genetic access to transiently active neurons via TRAP: targeted recombination in active populations. Neuron *78*, 773–784. https://doi.org/10.1016/j.neuron.2013.03.025.

69. Ye, L., Allen, W.E., Thompson, K.R., Tian, Q., Hsueh, B., Ramakrishnan, C., Wang, A.C., Jennings, J.H., Adhikari, A., Halpern, C.H., et al. (2016). Wiring and molecular features of prefrontal ensembles representing distinct experiences. Cell *165*, P1776–P1788. https://doi.org/10.1016/j.cell.2016.05.010.

70. Li, J., Jiang, R.Y., Arendt, K.L., Hsu, Y.T., Zhai, S.R., and Chen, L. (2020). Defective memory engram reactivation underlies impaired fear memory recall in Fragile X syndrome. eLife *9*, e61882. https://doi.org/10.7554/eLife.61882.

STAR★METHODS

KEY RESOURCES TABLE

REAGENT or RESOURCE	SOURCE	IDENTIFIER
Antibodies		
Rabbit anti c-fos	Santa Cruz Biotechnology	Cat#: sc-253 RRID:AB_2231996
Rabbit anti c-fos	Synaptic Systems	Cat#: 226 003 RRID:AB_2231974
Rabbit anti-pCREB	Cell Signaling Technology	Cat#: 9198 RRID:AB_2561044
Rabbit anti-pERK	Cell Signaling Technology	Cat#: 9101 RRID: AB_331646
Rabbit anti-Arc	Synaptic Systems	Cat#: 156002 RRID:
Mouse anti-Neun	Millipore	Cat#: MAB377 RRID:AB_2298772
Rabbit anti-PV	Swant biotechnologies	Cat#: PV27a −2014 RRID:AB_2631173
Mouse anti-Syt2	Zebrafish International Resource Center	Cat#: ZDB-ATB-081002-25
Goat anti-Mouse Alexa Fluor 405	Thermo Fisher Scientific	Cat#: A-31553, RRID:AB_221604
Goat anti-Mouse Alexa Fluor 488	Thermo Fisher Scientific	Cat#: A-710369, RRID: AB_2532697
Goat anti-Rabbit Alexa Fluor 647	Thermo Fisher Scientific	Cat#: A-21245, RRID:AB_141775
Bacterial and virus strains		
rv:CAG-FLEX-mCherry	Óscar Marín Lab	N/A
AAV9-CBA-FLEX-PSAM(Leu141Phe, Tyr115Phe)GlyR-WPRE	Vector Biosystems Inc	N/A
AAV-8/2-hSyn1-dlox-hM4D(Gi)_mCherry (rev)-dlox-WPRE-hGHp(A)	Viral Vector Facility Zurich	Cat#: v84-8
AAV-8/2-hSyn1-dlox-hM3D(Gq)_mCherry (rev)-dlox-WPRE-hGHp(A)	Viral Vector Facility Zurich	Cat#: v89-8
AAV-retro/2-hSyn1-chI-dlox-GtACR2_EGFP(rev)-dlox-WPRE-SV40p(A)	Viral Vector Facility Zurich	Cat#: v477-retro
AAV-9/2-c-Fos-chI-hERT2_iCre_hERT2(c.-d.)-WPRE-bGHp(A)	Viral Vector Facility Zurich	Cat#: v579
AAV-9/2-hEF1α/hTLV1-Coff/Fon(hM4D(Gi)_mCherry)-WPRE-hGHp(A)	Viral Vector Facility Zurich	Cat#: v779-9
AAV-DJ/2-hEF1α/hTLV1-Con/Fon(hM4D(Gi)_mCherry)-WPRE-hGHp(A)	Viral Vector Facility Zurich	Cat#: v870-DJ
Chemicals, peptides, and recombinant proteins		
NaCl	Sigma Aldrich	Cat#: S9888
KCl	Sigma Aldrich	Cat#: P3911
NaH_2PO_4	Roth	Cat#: 4984.1
$NaHCO_3$	Sigma Aldrich	Cat#: S6297
D-Glucose	Sigma Aldrich	Cat#: G7528
$CaCl_2$	Acros Organics	Cat#: 349615000
$MgCl_2$	Roth	Cat#: KK36.2
Choline chloride	Sigma Aldrich	Cat#: C1879
Na-ascorbate	Sigma Aldrich	Cat#: 11140

(*Continued on next page*)

Continued

REAGENT or RESOURCE	SOURCE	IDENTIFIER
Na-pyruvate	Sigma Aldrich	Cat#: P2256
K-gluconate	Sigma Aldrich	Cat#: G4500
HEPES	Sigma Aldrich	Cat#: H3375
Mg_2-ATP	Sigma Aldrich	Cat#: A9187
Na-GTP	Sigma Aldrich	Cat#: G8877
Na_2-phosphocreatine	Sigma Aldrich	Cat#: P7936
RNAseOUT	Invitrogen	Cat#: 10777019
Triton X-100	Sigma Aldrich	Cat#: T8787
dNTP mix	Invitrogen	Cat#: R0192
ERCC RNA Spike-In Mix	Thermo Fisher Scientific	Cat#: 4456740
PSEM308	Apex Scientific	N/A
Clozapine N-Oxide	Tocris	Cat#: 4936/10
Muscimol	Tocris	Cat#: 0289
T-5224	MedChemExpress	Cat#: HY-12270
4-Hydroxytamoxifen	Sigma Aldrich	CAS Number: 68392-35-8 Cat#: H6278
Sunflower oil	Sigma Aldrich	CAS Number: 8001-21-6 Cat#: 47123
BSA	Roth	Cat#: 8076.2
L-NAME	Abcam	Cat#: ab120136
EdU (5-ethynyl-2′-deoxyuridine)	ThermoFisher Scientific	Cat#: A10044
Click-iT™ Plus EdU Cell Proliferation Kit (488 nm)	ThermoFisher Scientific	Cat#: C10637
Prolong Gold antifade Mountant	ThermoFisher Scientific	Cat#: P36934
Experimental models: Organisms/strains		
Mouse: PV-Cre: 129P2-Pvalbtm1(cre)Arbr/J	The Jackson Laboratory	Cat#: 008069 RRID:IMSR_JAX:008069
Mouse: PV-FlpO: B6.Cg-Pvalbtm4.1(flpo)Hze/J	Silvia Arber Lab	Madisen et al.[44]
Mouse: C57BL6/J	Janvier Labs	N/A
Mouse: Lsi1: CB6-Tg(T1-mGFP21) 25PC	In house	Deguchi et al. [36]
Mouse: Lsi2: CB6-Tg(T1-mGFP15)	In house	Deguchi et al. [36]
Mouse: Syt2-Cre: C57BL/6-(SYT2-Cre)	In house	N/A
Mouse: TRAP2: Fostm2.1(icre/ERT2)Luo/J	The Jackson Laboratory	Cat#: 030323 RRID:IMSR_JAX:030323
Software and algorithms		
Imaris v9.2: Image processing software	Oxford Instruments	https://imaris.oxinst.com/packages?gclid=CjwKCAjwr8zoBRA0EiwANmvpYD2UHOibhjfPLDE074V784P-cpysglHy6bE5eremel-nGDKBkMGzdxoCurgQAvD_BwE RRID:SCR_007370
XUVStitch v1.8.1-beta5	Free Software Foundation Inc.	http://lmb.informatik.uni-freiburg.de/lmbsoft/xuvtools/ RRID:SCR_005894
GraphPad Prism 9	GraphPad software	https://www.graphpad.com/scientific-software/ RRID:SCR_002798
ZEN2010	Carl Zeiss AG	https://www.zeiss.com/microscopy/int/products/microscope-software/zen.html RRID:SCR_013672

(*Continued on next page*)

Continued

REAGENT or RESOURCE	SOURCE	IDENTIFIER
Intan RHD USB interface	Intan Technologies	https://intantech.com/ RRID:SCR_019278
Bonsai	NeuroGEARS Ltd.	https://bonsai-rx.org RRID:SCR_017218
MATLAB (v2022b)	Mathworks	https://www.mathworks.com/ RRID:SCR_001622
CellExplorer	Petersen et al. [50]	https://cellexplorer.org/ RRID:SCR_022358
Viewer2	Biobserve	N/A
Custom code for analysis of electrophysiology	This study	https://doi.org/10.5281/zenodo.15878942
Other		
Fibreoptic Cannula: MFC_200/250-0.66_4mm_ZF1.25(G)_FLT	Doric Lenses	https://doriclenses.com/
ASSY-116-H10b probes	Cambridge NeuroTech	https://www.cambridgeneurotech.com/

EXPERIMENTAL MODEL AND SUBJECT DETAILS

Mice

PV-Cre mice (129P2-Pvalbtm1 (Cre)Arbr/J) were obtained from Jackson Laboratory (Maine, USA). *PV-FlpO* (B6.Cg-Pvalbtm4.1(flpo) Hze/J) mice were kindly provided by Professor Silvia Arber (Friedrich Miescher Institute). C57Bl6/J mice were from Janvier Labs (Le Genest-Saint-Isle, France). Lsi1 (CB6-Tg(T1-mGFP21) 25PC) and Lsi2 (CB6-Tg(T1-mGFP15)) lines were previously generated in house.[36]

Syt2-Cre mice were generated in house using a CRISPR/Cas9 approach. The annotated genomic sequence of the *Synaptotagmin 2* gene was downloaded from ensembl genome browser and the 3′UTR contained in the exon 9 was selected as a target region for cut by the Cas9 protein. The sgRNA was selected among other candidates based on the low off target score provided by the crispr.mit.edu software. A donor cassette containing an internal ribosome entry site, a Cre recombinase and an SV40 polyadenylation site and flanked by a 1kb homology region on both ends was synthesized by a commercial vendor and injected intracytoplasmic at 10ng/μL into a donor C57BL6 zygote together with the following reagents: crRNA.

([mC][mG][mG]CCGGGGCCACGCCCCUAGUUUUAGAGCUAUGCUGUU[mU][mU][mG]) 300ng/μL (9μL), tracrRNA 65ng/μL (1μL), mRNA Cas9 (Sigma-1EA) 100ng/μL (6μL) in a total volume of 30μL.

Syt2-Cre were bred with *PV-FlpO* and double-positive offspring (Cre^+/Flp^+ mice) were used to target $Syt2^-PV^+$ cells.

Syt2-Cre, *PV-Cre* and *Syt2-Cre/PV-FlpO* mice were bred with Lsi1 and Lsi2 lines to evaluate the effect of manipulating PV^+ interneuron subpopulations in ensemble allocation.

All behavioral procedures on mice were approved by the Veterinary Department of the Kanton Basel-Stadt. Mice of 2.5–3.5 months of age at the start of behavioral procedures were used. Experiments were carried out with male mice aged 2.5–3.5 months at the onset of the experiment. In a small minority of experiments (inhibition of Syt2+ cells 15′ after cFC acquisition, with virus incubation at 28d; inhibition of Syt2-cells 3h after water-FOR) 1–2 female littermates were also used, as no sex specific difference could be detected in the level of performance, but nonetheless making sure that male and females were counterbalanced in each experimental group. Mice of the desired genotype and closely comparable age were assigned randomly to experimental groups. Controls from individual experiments are represented in respective graphs, and independent cohorts of mice were used for each experiment as presented in the graphs with individual black dots. Mice from separate cohorts and experiments were only pooled when they belonged to the exact same type of experiment. Mice of the desired genotype and closely comparable age were assigned randomly to experimental groups. Animals had access to water and food *ad libitum* and were single-housed 2–3 days prior to the onset of the experiments.

METHOD DETAILS

Retrovirus production and purification

The Cre-dependent, mCherry-expressing retroviral construct used to label early- or late-born PV + cells at birth date was kindly provided by Óscar Marín (King's College London). The vector was used to produce Moloney murine leukemia viruses (MoMLV) by transfection of HEK293T cells with CMV-vsvg and CMV-gagpol. Viral particles were obtained by collection of the media in which cells were cultured, concentration by ultracentrifugation and resuspension in PBS.

In utero injections

Pregnant *PV-Cre* females were anesthetized and embryos (E9.5 or E13.5 for early- or late-born PV + cells targeting, respectively) exposed. Retrovirus was injected through a beveled glass micropipette in the ventricles of the embryos.[41] The injection area was visualized using an ultrasound scanner (VisualSonics Vevo 770).

Acute brain slice and single cell collection for Smart-seq

Adult (P60), retrovirus-injected *PV-Cre* mice were deeply anesthetized with thiopental and transcardially perfused with 5mL of ice-cold, 5%CO_2-95%O_2-saturated, artificial cerebrospinal fluid (ACSF), containing (in mM): 125 NaCl, 2.5 KCl, 1.25 NaH_2PO_4, 26 $NaHCO_3$, 26 D-Glucose, 1 $CaCl_2$, 2 $MgCl_2$. Brains were extracted and cut using a vibratome in 350 mm slices in ice-cold, 5%CO_2-95%O_2-saturated cutting solution containing (in mM): 110 Choline chloride, 7 $MgCl_2$, 11.6 Na-ascorbate, 3.1 Na-pyruvate, 2.5 KCl, 1.25 NaH_2PO_4, 0.5 $CaCl_2$, 25 $NaHCO_3$, 25 D-Glucose. Slices were briefly rinsed in room temperature ACSF and then incubated in ACSF at 34°C for 30 min. Slices were then transferred to a submersion chamber constantly perfused with room temperature ACSF and retrovirally labeled cells were visually identified using fluorescence from the mCherry expressed by virus-infected PV^+ cells. Pipettes (1–2 MΩ resistance) filled with internal solution containing, in mM: 115 K-gluconate, 5 KCl, 10 HEPES, 10 Mg-ATP, 0.3 Na-GTP, 10 Na_2-phosphocreatine, were used to collect cells. Once harvested, the tip of the pipette was withdrawn, broken against the bottom of a PCR tube containing 5ul of Smart-seq2 lysis buffer containing 4 Units of RNAseOUT, 0.2% Triton X-100, 10 mM dNTP mix, 1:500000 ERCC spike-ins and 10 mM Smart-seq oligo dT (5′-AAGCAGTGGTATCAACGCAGAGTACT30VN-3′), and immediately frozen on ice. A total of 22 retrovirally-labelled cells were collected (11 early- and 11 late-born PV^+ cells).

Single-cell cDNA library preparation (Smart-seq2)

Cell lysate tubes were briefly spun and placed on ice until reverse transcription. Reverse transcription was performed immediately using Smart-seq2 chemistry with template-switching, as described.[42] First-strand cDNA synthesis was primed by the oligo-dT primer, and template-switch oligonucleotides were added to capture full-length transcripts. This was followed by 18 cycles of PCR pre-amplification of cDNA following the Smart-seq2 protocol. All reverse transcription and amplification steps were carried out according to the published Smart-seq2 protocol, with identical thermal cycling conditions and enzyme concentrations as reported.[42] Quality and yield of cDNA were assessed by measuring concentration (Qubit HS DNA assay) and size distribution (Agilent Bioanalyzer). For sequencing library preparation, the purified cDNA was augmented and indexed. Illumina sequencing libraries were generated from each single-cell cDNA (e.g., using Nextera XT or equivalent kits, following manufacturer's instructions). Indexed libraries were pooled equimolarly and subjected to high-throughput sequencing on an Illumina platform. Paired-end sequencing (2 × 75 bp or 2 × 100 bp reads) was performed to ensure full coverage of cDNA amplicons. The Illumina run produced raw FASTQ files for each cell, which were demultiplexed using unique index barcodes.

Sequencing data processing and bioinformatic analysis

Primary processing of single-cell RNA-seq data was conducted using the Galaxy platform. The analysis workflow included the following steps: Data Import and Quality Control: Raw sequencing reads (FASTQ files) from each cell were uploaded to Galaxy. Read quality was assessed using FastQC, and Illumina adapter sequences were removed (Trim Galore/Cutadapt) with a Phred quality cutoff of 20. Reads shorter than 20 nt after trimming were discarded to eliminate low-quality fragments. Read Alignment: High-quality trimmed reads were aligned to the mouse reference genome (mm10 build) using a splice-aware aligner (HISAT2 or STAR) with default parameters. The aligner indexed the reference genome and produced sorted BAM files for each single cell, containing the genomic alignments of the reads. Gene expression levels were quantified from the alignment files. Using genome annotation (Ensembl). ERCC Spike-in Normalization and QC: Reads mapping to the External RNA Controls Consortium (ERCC) spike-in transcripts were quantified in each cell. ERCC counts were used to evaluate the RNA capture efficiency and sensitivity, as each cell on average yielded detection of ∼10–15% of spike-in molecules. The transcript count data were then normalized for sequencing depth, using size factors or counts-per-million scaling, with adjustments informed by ERCC recovery. Quality control metrics (total reads, number of genes detected, ERCC recovery rate) were computed for each cell. Cells with poor ERCC detection were excluded from downstream analysis to ensure high-quality data. Data Normalization: The filtered gene count matrix was normalized to account for differences in coverage across cells. We applied a global scaling normalization (each cell's counts scaled to a fixed library size) to obtain normalized expression values. Differential Expression Analysis: To compare early-born versus late-born PV neuron populations, differential gene expression analysis was carried out between the two groups of single-cell transcriptomes. Using the normalized count data. All bioinformatic analyses were performed on the Galaxy platform and associated tools with default settings unless otherwise specified.

Stereotaxic surgery

Stereotaxic surgeries were performed using a stereotaxic alignment device (Model 1900, David Kopf Instruments). Briefly, mice were anesthetized using an OXYMAT3 and isoflurane (4–5% for induction, 1–2% for maintenance). Depth of anesthesia was repeatedly evaluated, and body temperature was maintained using a heating pad. Virus and intra-cerebral drugs delivery was performed using glass pipettes connected to a Picospritzer (Parker Hannifin). Injections were bilateral and viral/drug injections were paired with saline/vehicle injected mice to account for surgery-related effects. In viral injections, depending on the target brain area, 200–250 nL were injected, at a pace of 50 nL/min per injection site. To prevent reflux or off-target infection, pipettes were left for 10 min at the injection site after viral delivery. Injections in dH were performed at the following coordinates relative to bregma: anteroposterior (AP) −1.7,

mediolateral (ML) ±1.85, dorsoventral (DV) −2.0 and −1.6 (half of total volume at each DV level). Injections in vH were performed at the following coordinates relative to bregma: AP -3.1, ML ±3.1, DV -3.5, −3.- and −2.4 (40%, 40% and 20% of the total volume at each DV level, respectively). The following viral constructs were used across experiments: PSAM Inhibitor virus: AAV9-CBA-FLEX-PSAM (Leu141Phe, Tyr115Phe)GlyR-WPRE (Vector Biosystems Inc); DREADDs Inhibitor virus: AAV-8/2-hSyn1-dlox-hM4D(Gi)_mCherry (rev)-dlox-WPRE-hGHp(A) (Viral vector facility, ETHZ), DREADDs Activator virus: AAV-8/2-hSyn1-dlox-hM3D(Gq)_mCherry(rev)-dlox-WPRE-hGHp(A) (Viral vector facility, ETHZ); Cre-OFF/Flp-On DREADDs Inhibitor virus (AAV-9/2-hEF1α/hTLV1-Coff/Fon (hM4D(Gi)_mCherry)-WPRE-hGHp(A)) (Viral vector facility, ETHZ), Cre-ON/Flp-ON DREADDs Inhibitor virus (AAV-DJ/2-hEF1α/hTLV1-Con/Fon(hM4D(Gi)_mCherry)-WPRE-hGHp(A)) (Viral vector facility, ETHZ); Optogenetic Inhibitor virus: AAV-retro/2-hSyn1-chI-dlox-GtACR2_EGFP(rev)-dlox-WPRE-SV40p(A) (Viral vector facility, ETHZ), TRAP2-iCre virus: AAV-9/2-c-Fos-chI-hERT2_iCre_hERT2(c.-d.)-WPRE-bGHp(A) (Viral vector facility, ETHZ).

In experiments involving viral injections mice were kept in their home cage for 10–14 days after surgery to allow for recovery and expression of the target proteins. Before behavioral experiments involving activation of effector proteins (e.g., DREADDs inhibitor), mice were anesthetized, and ligands were delivered intraperitoneally (ip) to achieve the desired drug concentration. Injections were paired with ligand injected control mice to account for off-target drug effects.

In experiments involving acute intracerebral injections of drugs to dH or vH, the same coordinates stated above were used. Muscimol (Tocris Bioscience, #0289) was dissolved in saline and bilaterally injected (0.02 μg/inj.site). The cFos inhibitor T-5224 (MedChemExpress HY-12270) was dissolved in 20% polyvinylpyrrolidone (PVP) and 10% DMSO and bilaterally injected (1.5 μg/inj.site).

Behavior

Contextual fear conditioning (cFC)

For cFC mice were placed in a conditioning context for 3 min and then received 5-foot shocks (1 s, 0.8 mA each) spaced by 30 s. After 24 h, mice were placed in the same context for 5 min and freezing was measured (first min excluded). Freezing was defined as immobility beyond respiration.

cFC extinction

In extinction experiments, mice were placed for 30 min in the conditioning context 24 h after acquisition. Freezing was evaluated in 5 min intervals (first min excluded). After 24 h, mice were placed again in the conditioning context for 5 min for the retention session and freezing was measured (first min excluded).

Familiar object recognition (FOR)

For FOR (also known as NOR) mice were placed in an open arena, where they were allowed to explore two identical objects for 10 min. After 24 h, mice were placed in the same arena, but with one of the original objects replaced by a new one. Mice were allowed to explore the objects for 5 min, and time spent exploring each object was measured. A discrimination index (DI) was calculated as follows:

$$DI = 100 * \frac{NET - FET}{NET+FET}$$

where NET is the time spent (in seconds) exploring the novel object whereas FET is the time spent exploring the familiar object.

FOR in context

For FOR in context mice were subjected to two FOR acquisition events separated by 24h. Each FOR acquisition event took place in different contexts (Context 1 and Context 2, respectively) and with different pairs of objects. Recall took place in Context 1, where mice were presented with one object they had encountered on the first FOR acquisition and one they had encountered on the second FOR acquisition. Discrimination index was calculated as in regular FOR experiments, with positive and negative values indicating, respectively, a preference for the object the mice had seen in the second and in the first FOR acquisition.

Memory ensemble tagging and reactivation

For tagging and reactivation experiments, TRAP2-iCre and DREADDs activator viruses (see above) were delivered bilaterally in vH. After 10 days, mice underwent a first memory acquisition (either cFC or FOR). After 30 min mice received an ip injection of 50 mg/kg 4-Hydroxytamoxifen (4-OHT, Sigma Aldrich H-6278) or vehicle (sunflower oil) to tag memory ensemble neurons. Mice were left in their home cage for 14 days to allow strong expression of DREADDs activator protein. On the day of the second memory acquisition (either cFC or FOR), mice were injected ip with CNO 30 min prior to behavior to activate the tagged memory ensemble neurons. After 24 h, mice underwent memory recall for the second acquisition without perturbation.

Trap2 virus and controls

The Trap2 virus strategy employed in this study uses the v579 virus constructed by vvf Zurich vector core facility based on the cFosTtA vector,[67] the Trap2 mouse[68] and a FosCh virus.[69] The FosCh viral approach has been successfully verified and used for activity-dependent tagging of cfos+ ensemble neurons.[69,70] This virus strategy involves, packaging in an AAV construct a minimal cFos promoter and regulatory element in intron-1 to capture with specificity cFos+ neurons upon activation during learning or light stimuli.[69] The ER-Cre-ER cassette under cFos promoter ensures reliable targeting of activity- and tamoxifen-dependent labeling of

ensemble neurons. In order to account for variation in injection efficiency across mice, Ye et al.[69] verified with a dual-color quantification using an activity independent (CamKII-EYFP) and activity dependent (Fos-ER-Cre-ER-tdTomato) labeling of projections from behaviorally defined neuronal populations from the same injection site, that both viruses infected cells with a stable relative ratio across mice, suggesting efficient labeling with the FosCh virus of behaviorally activated ensemble neurons. Li et al.,[70] verified that vehicle injection showed minimal labeling and hence minimal expression leakage in neurons activated by experience. Furthermore, mice post enrichment experience showed significantly increased labeling with FosCh virus, as compared to their home cage control counterparts, indicating successful tagging of activated neuronal population with the viral approach.[70] The Trap2 virus used in the present study, was previously employed to label neuronal population encoding cFC learning in ventral hippocampus and Prelimbic cortex.[48] Labeled neurons were reactivated in neutral context to show efficient expression of fear in an unconditioned context; by contrast, mice injected with virus but not administered tamoxifen upon cFC, did not show fear expression upon reactivation with ligand injection. Additionally, home cage controls were injected with the virus and reporter but not administered tamoxifen to check for leakage expression, and no expression of the Trap2 virus was observed suggesting no leaky expression in the basal neuronal population.[48] These studies verified successful recruitment and activation of cfos+ neurons labeled with the Trap2 virus.

In the present study, Trap2 virus labeling was validated in home cage controls and post cFC, where significant increase in labeled cells was observed post cFC as compared to the home cage controls.

Optogenetic inhibition of Syt2$^+$PV$^+$ neurons

For optogenetic inhibition experiments, optogenetic inhibitor virus (see above) was injected bilaterally in vH and subsequently an optic fiber was implanted 100 μm above the injection site (MFC_200/250-0.66_4mm_ZF1.25(G)_FLT Mono Fibreoptic Cannula, Doric Lenses).

Optogenetic inhibition of Syt2$^+$PV$^+$ cells through excitation of GtACR2 in these cells was performed at different time intervals (see Figure 2D). Illumination (488 nm) was controlled using Radiant software (Plexon) and excitation intensity was maintained at 10 mW.

Interference with Lsi PN synaptogenesis in hippocampal vCA3

The nNOS inhibitor L-NAME (N^{ω}-Nitro-L-arginine methyl ester hydrochloride) was injected subcutaneously at 60mg/kg bodyweight. For repeated injections, the time interval between subsequent injections was 24 h. The drug was injected at either P5-7 (Lsi1 CA3 synaptogenesis), P7-9 (Lsi2 CA3 synaptogenesis) or P10-12. Analyses of the effect of L-NAME in synaptogenesis were performed either 24 h after the last injection (i.e., P8 or P10) or in adult animals. Subsequent behavioral and cFos expression analyses were performed as described for the other experiments in the study.

Connectivity analyses in nNOS inhibition experiments

For selective connectivity analysis between DG and CA3, the procedure was followed as in Deguchi et al., 2011. Briefly, contacts between presynaptic mGFP-positive Lsi1 (or Lsi2) mossy fiber terminals and mGFP+ Lsi1 (or Lsi2) or mCherry+ (randomly labeled with Rabies-mCherry, kind gift of S. Arber, Univ. of Basel) postsynaptic CA3b pyramidal neurons were analyzed. Fixed brains were embedded in 3% agarose gel and ca. 100 μm transverse hippocampal sections were collected for the analysis. Fluorescent dendrites with their entire dendritic tree within the section in stratum lucidum were monitored for individual LMTs and average distances between all labeled LMTs along one dendritic tree were computed. We considered as putative contact sites only events in which the distance between mossy fiber terminals (>3 μm diameter) and pyramidal neuron dendrites was smaller than 0.2 μm. Distance between consecutive contact sites in stratum lucidum was measured using Imaris for each CA3 pyramidal neuron.

In vivo electrophysiology

For *in vivo* electrophysiological recordings, a silicon probe mounted on picodrive (Cambridge NeuroTech Inc.) was implanted into vH in one of the hemispheres. Probe placement and location of recording sites were validated by an electrolytic lesion made using the channels at the top and bottom of the silicon probe. LFP were recorded on an Intan RHD USB interface board, and high-speed video data were collected at the same time logging the timestamps of each frame using Bonsai (v2.3, NeuroGEARS Ltd.). Preprocessing of LFP data involved manual curation of recorded channels to remove noisy/broken channels, z-scoring over the entire recording session and common-mode referencing across channels. The electrophysiological signal was processed using the interactive toolbox of CellExplorer and further using custom written MATLAB script (https://github.com/bhankoma/Valbuena-et-at-2015.git). The LFP analyses presented were averages of 5 channels per mouse. At water-FOR acquisition (day1), LFP was analyzed across 5min time intervals before FOR acquisition referred to as baseline, and post FOR acquisition at 8-13min, 17-22min and 28-33min. To compute the shift in LFP power from before to after FOR acquisition during the memory allocation windows, we subtracted the baseline LFP oscillations from the timepoints post FOR acquisition. Mean low- and high-gamma frequency values were averaged across the 31–55 Hz, and 55–100 Hz range, respectively.

Immunohistochemistry

The following antibodies and concentrations were used: rabbit anti-cFos (Santa Cruz Biotechnology sc-253 1:1000 and Synaptic Systems 226003 1:1000), rabbit anti-pCREB (Cell Signaling Technology 9198, 1:1000), rabbit anti-pERK (Cell Signaling Technology 9101, 1:800), rabbit anti-Arc (Synaptic Systems 156 002, 1:500), mouse anti-NeuN (Millipore MAB377 1:1000) rabbit anti-PV (Swant

PV27a-2014, 1:5000), mouse anti-Syt2 (ZIRC, ZDB-ATB-081002-25, 1:200), Alexa 405 conjugated anti-mouse (ThermoFisher Scientific A31553 1:1000), Alexa 488 conjugated anti-mouse (ThermoFisher Scientific A710369 1:1000) and Alexa 647-conjugated goat anti-Rabbit IgG (ThermoFisher Scientific A21244 1:1000).

For quantification of plasticity marker (cFos, pERK, pCREB, Arc) expression induced upon learning, mice were transcardially perfused with 4% PFA in PBS (4°C, pH 7.4) at defined time points (15, 30, 45, 60 or 90 min) after the end of a behavioral paradigm (cFC or FOR acquisition or recall). Brains were kept in 4% PFA at 4°C for 16-18h before being rinsed with PBS and cut into 40 mm coronal slices using a vibratome. Slices were blocked with 10% bovine serum albumin (BSA, Roth 8076.2) in PBS-T (0.3% Triton X-100 in PBS) and immunostained with primary antibody in 3% BSA PBS-T overnight at 4°C. Sections were washed in PBS-T three times (10 min each) and incubated with secondary Alexa 647-conjugated anti-rabbit antibody for 2h. After three washing steps, slices were mounted with Prolong Gold antifade Mountant (ThermoFisher Scientific P36934) and kept at 4°C. Imaging was performed using either a Zeiss LSM-700 confocal microscope or a Zeiss Axio Imager M2 equipped with a spinning disk confocal scanning unit Yokogawa CSU W1 with Dual T2. Images obtained with any of the two microscopes yielded equivalent results. Samples from the same experiment were imaged and analyzed in parallel using the same settings. Image mosaics were generated using XUVStitch (v1.8.1-beta5, Free Software Foundation Inc.) or an in-house developed ImageJ plugin and analysis was performed using Imaris software (version 9.2). Cells positive for plasticity markers were automatically detected using spot detection in Imaris with a cell radius parameter of 10 μm and total marker expression obtained by normalization over $NeuN^+$ cells. Marker expression in Lsi1 and Lsi2 neurons was quantified as the percentage of GFP^+ cells with a $marker^+$ nucleus.

For PV expression analysis, the zero value was set at pyramidal neuron somas, and the highest threshold was set so that less than 20% of pixels belonging to the brightest PV^+ cells were saturated. PV^+ interneuron somas were isolated using 3D isosurfaces detection in Imaris and raw per-cell average intensities were plotted as single-neuron arbitrary intensity units in GraphPad Prism v10 (GraphPad Software, La Jolla, USA). Categories for PV^+ cells PV expression were defined as previously described (Donato et al., 2013).

Birthdating experiments

EdU (5-ethynyl-2′-deoxyuridine, ThermoFisher Scientific) labeling at defined time points in pre-natal development was used to validate the early-born nature of PV cells targeted with Syt2-Cre mice. EdU 5 mg/kg was injected IP in Syt2-Cre pregnant female mice at the indicated day post-fertilization (E9.5 to E14.5 range). Offsprings were injected into vH with a Cre-dependent fluorescent reporter to identify Syt2+ cells. Animals were transcardially perfused 10 days after surgery. Brains were subsequently processed for PV immunostaining (see above) and EdU was detected using the Click-iT Plus EdU Cell Proliferation Kit (488 nm, ThermoFisher Scientific).

QUANTIFICATION AND STATISTICAL ANALYSIS

All statistical analyses were performed using GraphPad Prism. Depending on the dataset, statistical groups were compared using Exact Mann-Whitney, unpaired Student's t-test, one-way ANOVA followed by Dunnett's or Turkey's multiple comparison post hoc test, or two-way ANOVA followed by Turkey's or Fisher's least significant difference multiple comparison post hoc test ($p < 0.05$). Average values are expressed as means ± S.E.M. Sample sizes per group are indicated by individual spots in the respective figure. Mice of the desired genotype and closely comparable age were assigned randomly to experimental groups. Initial pilot experiments with 3 mice each comparing means of control, $Syt2^+PV^+$ and $Syt2^-PV^+$ for different behavioral and imaging analysis experiments, had a calculated Cohen's d value for effect size above 3.5. Using this effect size d value, a power of 0.9, alpha error = 0.05. and two tailed tests we obtained a minimal sample size per group of $n = 4$, for Student's t-test and ANOVA tests, to reject the null hypothesis. Accordingly, we have used $n \geq 4$ mice for each condition whenever possible. For the LFP analysis our pilot experiments an effect size d value of 2, and hence a minimum sample size per group of $n = 2$. Accordingly, for these analyses the sample size was $n = 2$.

Cell Reports, Volume *44*

Supplemental information

Early time window for memory ensemble allocation specifically depending on activity in Syt2+ early-born parvalbumin interneurons

Sergio Valbuena, Komal Bhandari, Annapoorani Udhayachandran, Matteo Tripodi, and Pico Caroni

Supplementary figure legends:

Fig. S1: Targeting early- and late-born PV interneuron subpopulations through Syt2 expression. Related to Fig. 1.
(**A**) Expression level comparison for selected gene groups in early- and late-born PV neurons. Enhanced expression of neurotransmission, fast-spiking and excitatory signaling genes in early-born PV neurons and of inhibitory signaling and actin dynamics genes in late-born PV neurons.
(**B**) Co-localization (arrows) between Syt2 (immunocytochemistry) and early-born PV cells (Cre-dependent mCherry virus) but not between Syt2 and late-born PV cells in dH. Bars: 5 μm.
(**C**) Representative examples of PV neuron labeling intensities in vCA1. Bar: 50 μm.
Exact Mann-Whitney test. $p < 0.05$ (*), $p < 0.01$ (**), $p < 0.001$ (***). n = 11.

Fig. S2: Early time window for Syt2+ PV-dependent memory formation. Related to Fig. 2.
(**A**) PSAM/PSEM chemogenetic system: impact of vH chemogenetic inhibition of Syt2+ PV cells 15 min (but not 30 min or 60 min) after cFC acquisition on freezing at recall.
(**B**) Injection site of viruses in vH and representative image of Syt2+ PV+ cells targeted with mCherry-DREADD.
(**C**) Inhibition of Syt2+/PV+ cells with DREADD 15 min after acquisition of cFC: CNO injection and virus (+/- Cre) controls.
(**D**) Chemogenetic inhibition of Syt2+/PV+ neurons using Cre-on/Flp-on system 15 min after cFC acquisition (freezing at recall).
(**E**) Chemogenetic inhibition of Syt2+ PV cells upon 28d of DREAD virus incubation (inhibition 15 min (but not 30 min) after cFC acquisition; freezing at recall).
(**F**) Impact of vH PV subpopulation chemogenetic inhibition at different times after acquisition (or during recall) of cFC on freezing at recall; comparison to inhibition of all PV+ neurons.
(**G**) Impact of dH or vH silencing through PV cells activation during cFC extinction on freezing during extinction learning or at retention.
Unpaired Student's t test (**A, D, E, F**). Ordinary Two-way ANOVA followed by Dunnett's multiple comparisons post-hoc test (**C**). Repeated measure two-way ANOVA followed by Turkey's multiple comparisons test (**G**, left plot). Ordinary One-way ANOVA followed by Turkey's multiple comparison post-hoc test (**G**, right plot). $p < 0.05$ (*), $p < 0.01$ (**), $p < 0.001$ (***), $p < 0.0001$ (****). n = 4-9 (**A**), 4-5 (**C, D, E, G**) 4-25 (**F**).

Fig. S3: Value-related early closing of time window for memory formation. Related to Fig. 3.
(**A**) Total exploration times of familiar (F) and novel (N) object during recall in representative FOR experiments with inhibition of PV+, Syt2-/PV+ or Syt2+/PV+ neurons.
(**B**) Memory recall in FOR and water-FOR experiments 7 days after acquisition.
(**C**) Memory formation in cFC is suppressed by delivery of cFos inhibitor 30 min before acquisition, but not 2.5h after acquisition.
Unpaired Student's t test (**A**). Ordinary Two-way ANOVA followed by Turkey multiple comparison post-hoc test (**C**). $p < 0.05$ (*), $p < 0.01$ (**), $p < 0.001$ (***), $p < 0.0001$ (****). n = 4-13 (A), 4 (B, C).

Fig. S4: vH network activity during Syt2+ -dependent memory time window closing. Related to Fig. 3.

(**A**) Left: schematic representation of LFP recordings in water-FOR protocol (left, bottom) and representative image of individual implant sites (left, top; blue dots) in vH. HC: home cage. Right: representative image of LFP power spectrum from CNO control mouse (water FOR), showing Power shifts during 32min, starting 1min before end of water access. Vertical line: 15 min timepoint at which CNO was injected.
(**B**) Power shift from baseline as a function of time after acquisition of water-FOR. Mean theta, low-gamma, and high-gamma band. Average values for 5 min time intervals in unperturbed mice as indicated.
(**C**) Impact of Syt2+ or Syt2- PV neuron inhibition at 15 min on power shift after water-FOR. Ordinary Two-way ANOVA followed by Tukey's repeated measure multiple comparison post-hoc test (**C**) $p < 0.05$ (*). n=2 (**B**), n=2-3 (**C**).

Fig. S5: Syt2+ -dependent selective allocation of cFos+ neurons into relevant Lsi1/2 subpopulations. Related to Figs. 4, 6.
(**A**) Home cage immunocytochemistry values (pCREB, pERK, Arc) and values 15 min after cFC (pCREB) in % of total Lsi1/2 PNs.
(**B, C**) PV neuron inhibition at 15 min (but not 3h) after cFC (**B**) or FOR (**C**) acquisition disrupts selective allocation of vH-CA1 cFos+ neurons to Lsi2 (**B**), or Lsi1 (**C**) PNs respectively. Detection upon cFC recall.
(**D**) Syt2+ PV neuron inhibition during recall of cFC (above) or FOR (below) does not disrupt selective allocation of vH-CA1 cFos+ neurons to Lsi2, or Lsi1 PNs respectively.
(**E**) Syt2+ (but not Syt2-) PV neuron inhibition at 15 min after cFC acquisition disrupts selective allocation of vH-CA1 cFos+ neurons to Lsi2 PNs. Detection 90 min after acquisition.
(**F**) Syt2+ PV neuron (or all-PV neuron) inhibition at 15 min after FOR acquisition disrupts selective allocation of vH-CA1 cFos+ neurons to Lsi1 PNs. Detection 90 min after acquisition.
(**G**) Top: Representative images of TRAP2-mouse- (left) and virus-mediated (right) tagging of ensemble cells in vCA1 upon cFC (white arrows indicate tagged cFos+ cells). Bar: 30um. Bottom: % overlap between cFos-tagged cells and cFos labeled cells at recall (left); % of tagged cells/NeuN+ in home cage or at acquisition of cFC (middle-left); % cFos+/NeuN+ in the home cage and upon cFC recall (middle right); same for FOR with TRAP2 virus (left panels).
Unpaired Student's t test (**A**, markers in Lsi1 vs Lsi2 cells; **B-F**, total cFos). Ordinary Two-way ANOVA followed by Fisher's least significant difference multiple comparison post-hoc test (cFos in Lsi1 and Lsi2 cells) (**B-F**). Ordinary One-way ANOVA followed by Fischer's least significant difference multiple comparison (**G**). $p < 0.05$ (*), $p < 0.01$ (**), $p < 0.001$ (***). n = 2-4 (**A**), 3-4 (**B**), 3-5 (**C**), 4-7 (**D, E**), 3-6 (**F**), 2-6 (**G**).

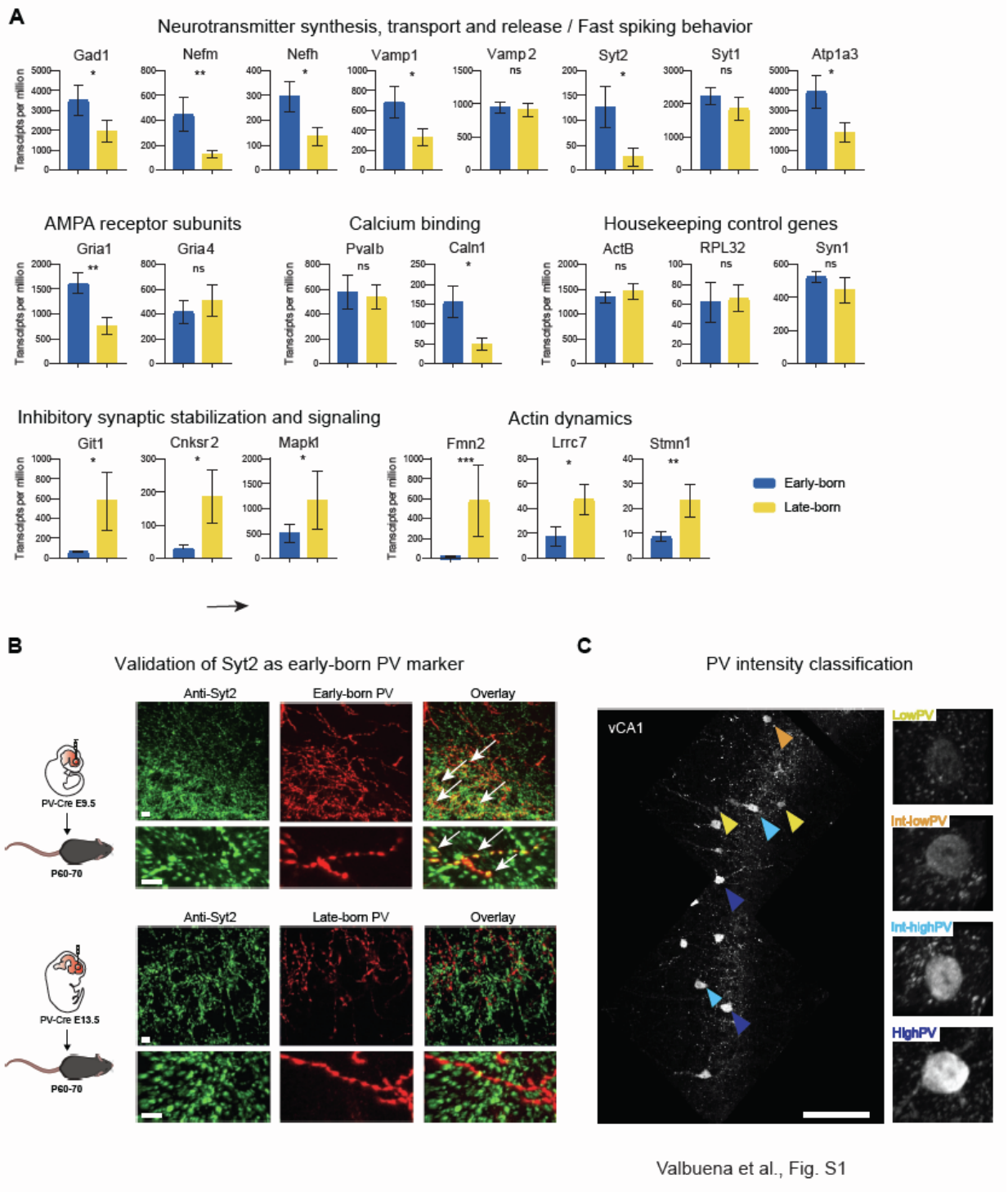

Valbuena et al., Fig. S1

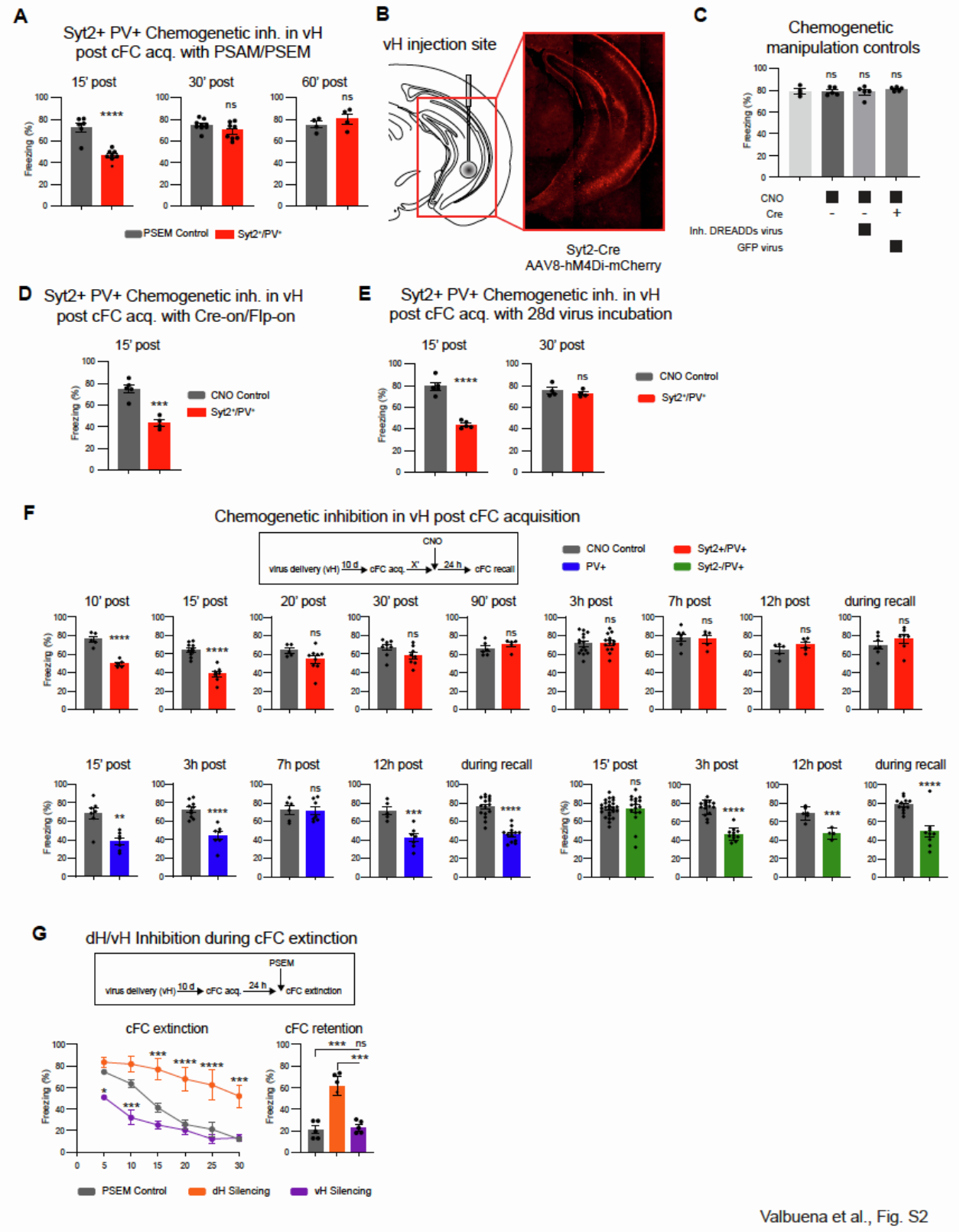

Valbuena et al., Fig. S2

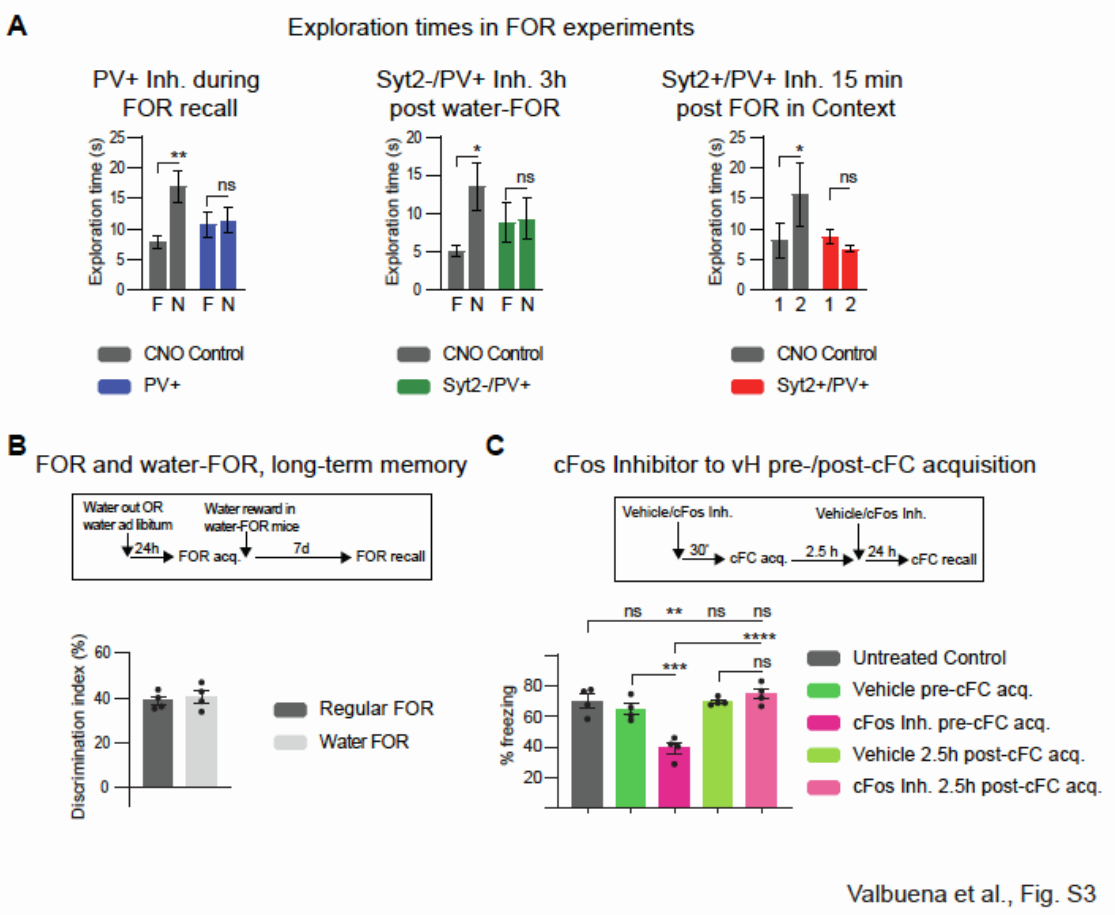

Valbuena et al., Fig. S3

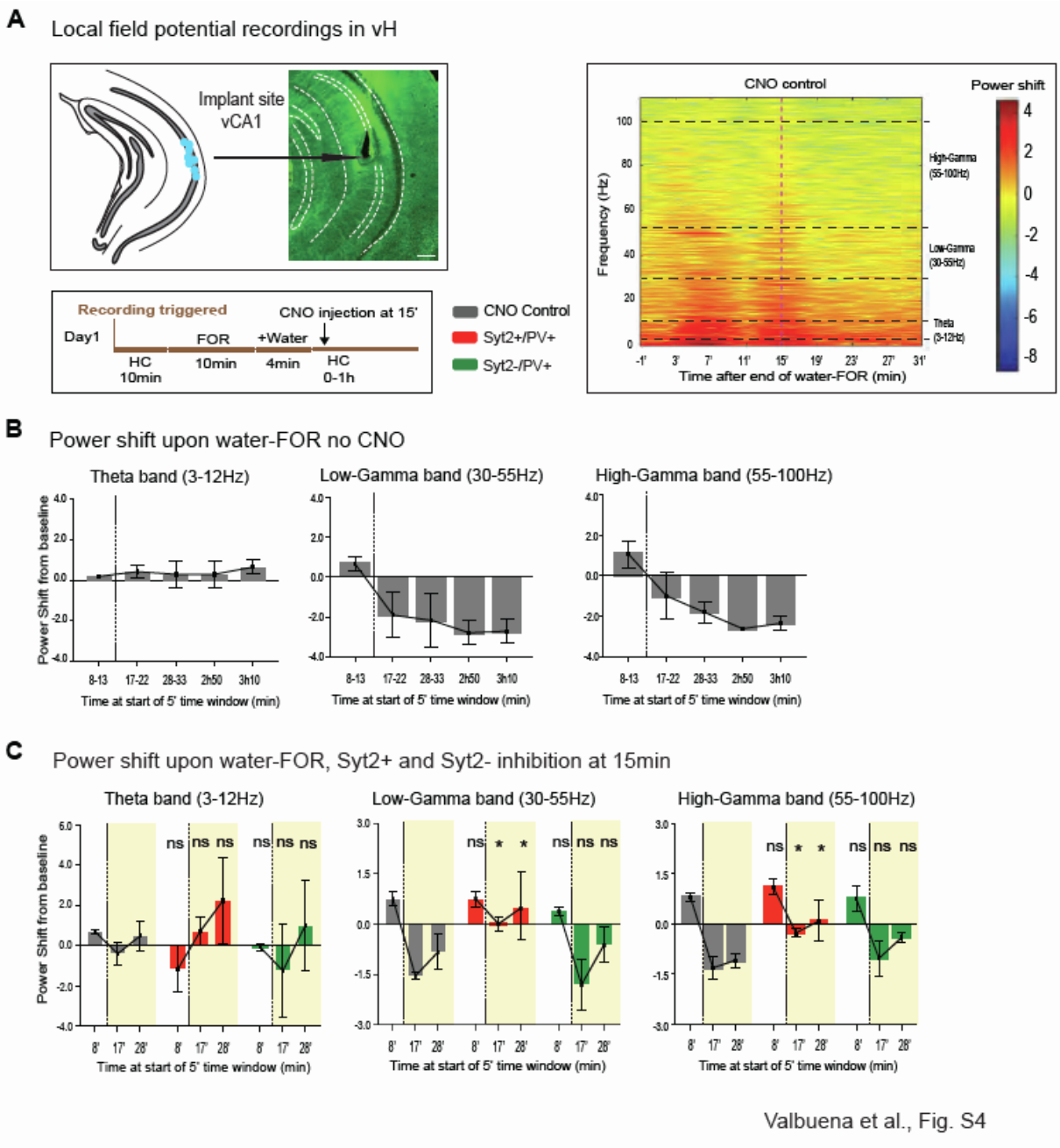

Valbuena et al., Fig. S4

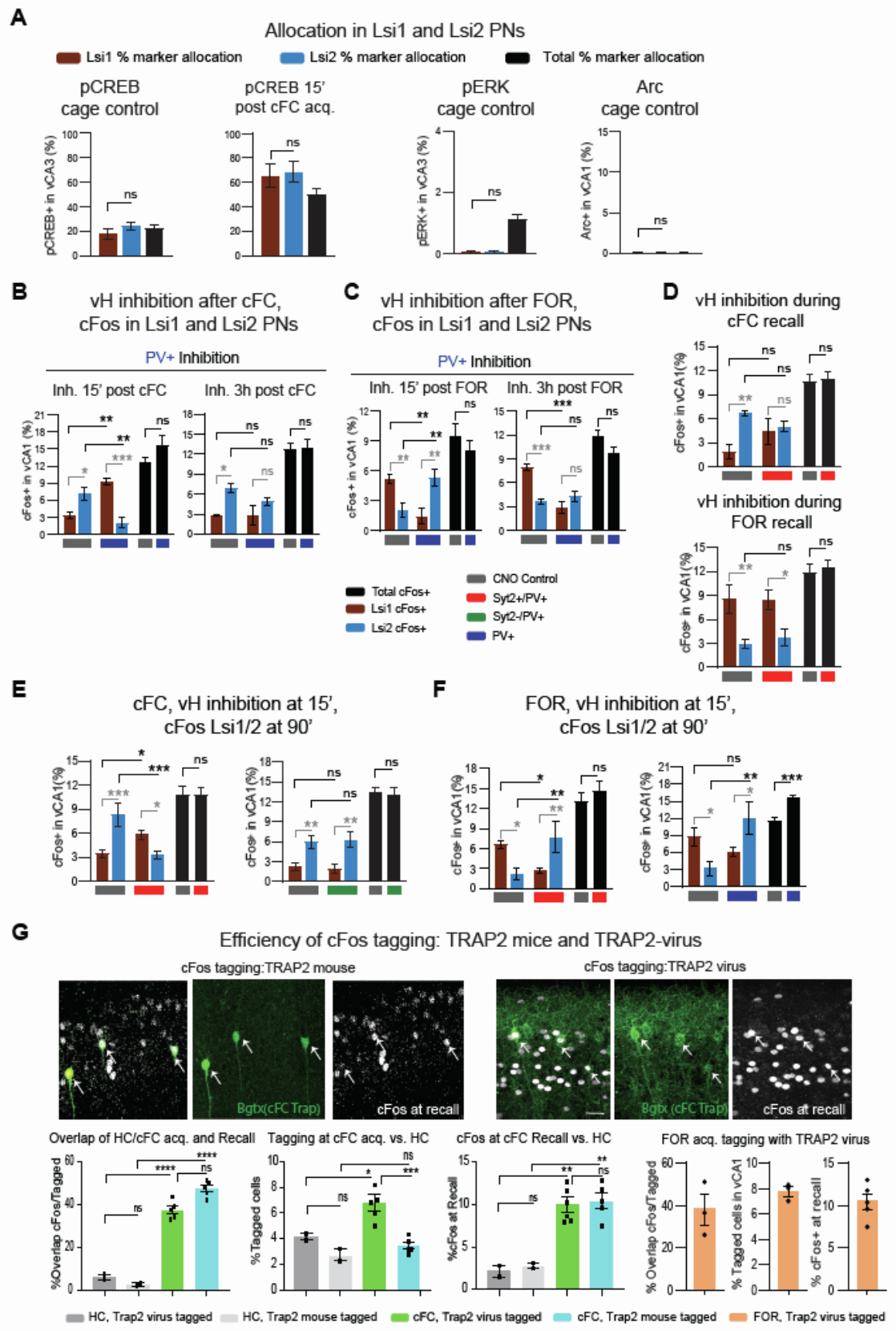

Valbuena et al., Fig. S5